Use of mine waste for H_2O_2-assisted heterogeneous Fenton-like degradation of tetracycline by natural pyrite nanoparticles

Catalyst characterization, degradation mechanism, operational parameters and cytotoxicity assessment

Mashayekh-Salehi, Ali; Akbarmojeni, Khatare; Roudbari, Aliakbar; van der Hoek, J.P.; Nabizadeh, Ramin; Dehghani, Mohammad Hadi; Yaghmaeian, Kamyar

DOI
10.1016/j.jclepro.2020.125235

Publication date
2021

Document Version
Final published version

Published in
Journal of Cleaner Production

Citation (APA)
Mashayekh-Salehi, A., Akbarmojeni, K., Roudbari, A., van der Hoek, J. P., Nabizadeh, R., Dehghani, M. H., & Yaghmaeian, K. (2021). Use of mine waste for H_2O_2-assisted heterogeneous Fenton-like degradation of tetracycline by natural pyrite nanoparticles: Catalyst characterization, degradation mechanism, operational parameters and cytotoxicity assessment. *Journal of Cleaner Production*, *291*, Article 125235. https://doi.org/10.1016/j.jclepro.2020.125235

Journal of Cleaner Production 291 (2021) 125235

Contents lists available at ScienceDirect

Journal of Cleaner Production

journal homepage: www.elsevier.com/locate/jclepro

Use of mine waste for H_2O_2-assisted heterogeneous Fenton-like degradation of tetracycline by natural pyrite nanoparticles: Catalyst characterization, degradation mechanism, operational parameters and cytotoxicity assessment

Ali Mashayekh-Salehi [a], Khatare Akbarmojeni [b], Aliakbar Roudbari [c], Jan Peter van der Hoek [d], Ramin Nabizadeh [b], Mohammad Hadi Dehghani [b], Kamyar Yaghmaeian [b, *]

[a] School of Public Health, Shahroud University of Medical Sciences, Shahroud, Iran
[b] Department of Environmental Health Engineering, School of Public Health, Tehran University of Medical Sciences, Tehran, Iran
[c] Center of Health Related Social and Behavioral Sciences Research Center, Shahroud University of Medical Sciences, Shahroud, Iran
[d] Delft University of Technology, Department of Water Management, Delft, the Netherlands

ARTICLE INFO

Article history:
Received 8 August 2019
Received in revised form
10 September 2020
Accepted 18 November 2020
Available online 23 November 2020

Handling editor: Prof. Jiri Jaromir Klemeš

Keywords:
Emerging contaminants
Tetracycline
Cell viability
Fenton-like
Pyrite
Mineralization
Sulfur defect

ABSTRACT

Degradation of tetracycline (TTC) with a heterogeneous Fenton-like pyrite/H_2O_2 process by pyrite from mine waste as a mineral catalyst was investigated. The study focused on identifying the main oxidizing agents and degradation mechanisms along with operational variables including solution pH, pyrite and H_2O_2 concentration, contact time, solution temperature, and initial TTC concentration. Catalyst characterization tests revealed that pyrite is a mesoporous powder with a high degree of FeS_2 purity. Radical scavenger tests demonstrated that $^{\bullet}OH$ was the main oxidizing agent generated by both solution and surface phase reactions. During the pyrite/H_2O_2 process, more than 85% of TTC was mineralized in 60 min and the maximum TTC removal was attained in the solution at an acidic pH value (4.1). The most abundant transformation products of TTC, formed by the attack of $^{\bullet}OH$ radicals, were simple chain carboxylic acids. Cultured cells of human embryonic kidney (HEK) were used for the cytotoxicity assessment of raw and pyrite/H_2O_2 treated TTC solutions. The results illustrated that the viability of HEK cells was enhanced considerably after treating TTC solutions under optimal conditions. Accordingly, pyrite originating from mine waste is a practically effective and cost-effective catalyst in heterogeneous Fenton-like systems for mineralization and degradation of emerging contaminants such as antibiotics.

1. Introduction

Antibiotics are among the emerging contaminants which are extensively being prescribed for the control of infectious diseases. There is a wide variety of antibiotics which are used with specific purposes (Awasthi et al., 2019; Pourakbar et al., 2016). Among antibiotic pharmaceuticals, tetracycline (TTC) is one of the extensively used drugs for clinical therapy and also for livestock industry (Liu et al., 2018; Ravikumar et al., 2019; Xu and Li, 2010). TTC is accounted for about 60% of the all antibiotics applied in the animal's therapeutics (Pereira et al., 2013). Properties such as vast-spectrum of antimicrobial activity against diverse infectious diseases, activity against both gram negative and positive bacteria, availability, and the low price are the reasons for extensive use of TTC (Shariati et al., 2009). On the other hand, imperfect metabolism in the human and animal body and incomplete pharmaceutical removal in conventional systems for wastewater treatment lead to the intrusion of TTC into the aquatic environment, with subsequently frequent detection in surface and ground waters, sediments and soils (Mboula et al., 2012). Presence of TTC in the environment is

* Corresponding author. Department of Environmental Health, School of Public Health, Tehran University of Medical Sciences, Tehran, Iran.
E-mail addresses: mashayekh@shmu.ac.ir (A. Mashayekh-Salehi), akbari.khatere72@gmail.com (K. Akbarmojeni), roodbari@shmu.ac.ir (A. Roudbari), j.p.vanderhoek@tudelft.nl (J. Peter van der Hoek), nabizadeh@tums.ac.ir (R. Nabizadeh), hdehghani@tums.ac.ir (M.H. Dehghani), mashayekh@shmu.ac.ir (K. Yaghmaeian).

https://doi.org/10.1016/j.jclepro.2020.125235
0959-6526/

threatening the public health and may lead to antibiotic-resistance of bacteria. Therefore, it is of great importance to remove TTC from contaminated flows prior to discharge it into the water resources.

Conventional water and wastewater treatment methods such as slow/high rate sand filtration, precipitation, flocculation/coagulation, activated carbon filtration, and chlorination have no sufficient capacity for the elimination of TTC from water (Ma et al., 2009; Shariati et al., 2009). In addition, TTC has toxic effects on conventional biological treatment processes (Li et al., 2016; Okoli and Ofomaja, 2019). Therefore, efforts to find efficient and new methods for treatment of water contaminated with TTC are urgently required.

Compared with conventional and traditional methods, advanced oxidation processes (AOPs) based on classical Fenton and Fenton-like processes have attracted the consideration of many scientists for treating recalcitrant and toxic organic pollutants, because of some unique advantages (Diao et al., 2017; Khataee et al., 2017). The classical Fenton reaction is based on the reaction of highly oxidizing agents, like $^{\bullet}OH$, in aqueous solution with the interaction of peroxides (mostly H_2O_2) and ferrous ions in acidic solution according to Eq. (1):

$$Fe^{2+} + H_2O_2 \rightarrow Fe^{3+} + OH^- + {}^{\bullet}O\,H \quad (1)$$

Hydroxyl radicals ($E^{\circ} = 2.8$ V) oxidize the organic substances by gaining an electron to form a hydroxide anion (redox reaction; Eq. (2)), or the organic compounds can be oxidized through dehydrogenation in which the hydroxyl radicals abstract a hydrogen atom from hydrocarbons (Eq. (3)), or the process proceeds via electrophilic addition to π systems (hydroxylation; Eq. (4)). Further oxidation of these intermediates via hydroxyl radicals leads to full mineralization of organic substances (Mirzaei et al., 2017; Nidheesh, 2015).

$$^{\bullet}O\,H + RX \rightarrow RX^{+\bullet} + OH^- \quad (2)$$

$$RH + {}^{\bullet}O\,H \rightarrow R^{\bullet} + H_2O \quad (3)$$

$$RHX + {}^{\bullet}O\,H \rightarrow RHX(OH) \quad (4)$$

The classic Fenton processes have been extensively used for treating wastewater containing refractory pollutants, due to its safe and environmentally-benign nature of reagents, simplicity, absence of mass transfer limitations, as well as short reaction times (Hermosilla et al., 2009; Mackuľak et al., 2015). However, there are some critical limitations such as narrow acidic pH ranges for operation, intense iron leach to the environment, demand of iron retrieve before the discharge within the guideline values (about 2 ppm) (Ghanbarian et al., 2017; Mirzaei et al., 2017), high H_2O_2 consumption, formation of huge amounts of iron-containing sludge, termination of the Fenton reaction and high operational costs (Bokare and Choi, 2014; Gao et al., 2015; Mirzaei et al., 2017). For these reasons, in recent years, the $^{\bullet}OH$ -based heterogeneous Fenton-like processes using solid Fe catalysts such as pyrite have received increasing consideration to overcome the main shortcomings of the conventional Fenton process (Diao et al., 2017). Pyrite (FeS_2) is found in hydrothermal deposits and is accounted as the most widespread sulfide mineral on earth. Mining for metals and coal is a common activity enhancing the exposure of pyrite to air, and hereby changing its oxidation level, although it is formed in anoxic environments. In many mines such as copper and zinc ore mines, pyrite is found as waste rock. Although no economic assessment was done in the present study, cost-effectiveness of waste pyrite as catalyst for aqueous pollutant solutions is confirmed by numerous researchers (Kantar et al., 2019c; Oral and Kantar, 2019). Therefore, use of this waste as a substance for wastewater treatment could be cost-effective and environmental-friendly.

Recent studies show that oxidation of pyrite in aqueous solutions with dissolved oxygen could generate H_2O_2 and $^{\bullet}OH$. Although pyrite can release H_2O_2 in the solution spontaneously, addition of extra hydrogen peroxide could accelerate its Fenton process properties (Cohn et al., 2006; Schoonen et al., 2010). To date, many studies have demonstrated that organic pollutants such as pharmaceutical compounds can be successfully degraded via pyrite in the heterogeneous Fenton-like process (Bae et al., 2013; Che et al., 2011; Gosselin et al., 2013; Labiadh et al., 2015). Although there is a large number of studies performed with raw pyrite from mining (Diao et al., 2017; Kantar et al., 2019b; Labiadh et al., 2015), there is no study evaluating the catalytic activity of mine waste pyrite in the pyrite Fenton process for degradation of TTC as a recalcitrant water pollutant. Also, the difference in the cytotoxicity of the raw pharmaceutical solution and treated effluent has not been checked in the studies using the pyrite Fenton process for degradation of pharmaceutical pollutants.

In the present study, a mine waste material, pyrite, was used as catalyst in the heterogeneous Fenton-like process for degradation of TTC as an emerging pollutant in water. The hypothesis is that pyrite-induced waste rock/mining material is at least as effective as pyrite originating from non-waste minerals and synthetic types for degradation of emerging organic pollutants in contaminated water. The aims of the present study are to (1) investigate the treatability of TTC containing solutions in a batch system by the pyrite-Fenton process, using pyrite from mine waste, (2) evaluate the effect of environmental factors including the pH of the solution, the nanocatalyst dosage, the initial TTC concentrations, the solution temperature, and the water matrix on TTC removal, (3) measure the mineralization of TTC by the pyrite-Fenton process, and (4) evaluate the cytotoxicity of the raw TTC solution and treated effluent.

2. Materials and methods

2.1. Chemicals and reagents

The chemicals used in this study are described in the Supplementary Information, SI (Text S1).

2.2. Preparation of pyrite nanoparticles and characterization

The natural pyrite catalyst was obtained from the Ahan-Lajaneh mine in Shahroud, Iran. Details of the nanocatalyst preparation can be found in SI (Text S2).

The prepared nanoparticles were characterized for surface morphology, chemical composition, crystalline shape, surface functional groups, structural composition and distribution of nanoparticles. Details of experimental techniques utilized for characterization of the nanopyrite catalyst are presented in SI (Text S3). The pH of point of zero charge (pHpzc) for the pyrite was determined according to the pH-drift procedure reported by Altenor et al. (2009).

2.3. Experimental procedure and analytical methods

TTC removal tests with the pyrite nanoparticles were performed in batch experiments in 100 mL flasks equipped with magnetic stirrers. In the experiments, 50 mL of TTC solution with a required initial concentration and pH was prepared by diluting the stock TTC solution with deionized water, which was subsequently transferred into a beaker on a magnetic stirrer. The solution pH was regulated by 1 N NaOH and HCl solutions. A predefined amount of

nanoparticles and/or predetermined H_2O_2 mass were then added to the solution, and the attained suspension was quickly stirred for a predetermined reaction time. The experimental parameters were investigated using operating conditions for the runs as given in Table S1. After the reaction time completion, the treated solution was filtered through a MCE Jet Biofil filter using a pore size of 0.22 μm, and the filtered solution was analyzed for the remaining TTC concentration. All experiments were performed in duplicate and the mean of two measurements was considered as the result.

In order to determine the TTC concentration, a HPLC (Agilent Co, C18 column) equipped with a UV detector at 358 nm was utilized. Details about the HPLC performance, along with evaluation procedures for the degradation and mineralization rate of TTC and catalytic activity of pyrite nanoparticles, are presented in SI (Text S4). Initial and final concentration of chemical oxygen demand (COD) were determined using the closed reflux procedure (ECO 8 Thermoreactor, COD analyzer, VELP SCIENTIFICA Company) according to Standard methods for the examination of water and wastewater (American Public Health Association (APHA), 2005).

2.4. By-products analysis

The nitrogen-based mineralization by-products were monitored by analyzing mineralized nitrogenous species including nitrate, nitrite, ammonium and total nitrogen using the procedure according to Standard methods for the examination of water and wastewater (American Public Health Association (APHA), 2005). The leached total iron concentration was measured by flame atomic absorption spectroscopy (FAAS).

A liquid chromatography/mass spectrometry instrument (LC/MS, Shimadzu, 2010 A) was used to detect TTC organic transmission products during the pyrite/H_2O_2 process. Details about the LC/MS performance are presented in SI (Text S5).

2.5. Cytotoxicity assessment

HEK 293 cells (human embryonic kidney cells) were purchased from National Cell Bank of Iran (NCBI) and cultured at 37 °C, 5% of carbon dioxide in Dulbecco's Modified Eagle's Medium (DMEM). The medium was supplemented with 10% heat-inactivated Fetal Bovine Serum (FBS) and penicillin/streptomycin 1% antibiotics in a humidified atmosphere containing 5% CO_2 at 37 °C. Cytotoxicity assessment was performed using the 3-(4,5-dimethylthiazol-2-yl)-2,5-diphenyltetrazolium bromide (MTT) assay. Details about MTT assay are presented in SI (Text S6).

3. Results and discussion

3.1. Catalyst characterization

The XRD patterns of the raw pyrite powder and pyrite powder after four successive catalytic reaction cycles are shown in Fig. S1. Some distinguished peaks were in good agreement with the structure of pyrite related to data files of the Joint Committee on Powder Diffraction Standards (JCPDS) diffraction (JADE 9, Materials Data Inc.) and matched well with the data of pyrite FeS_2 (Bae et al., 2013; Zhang et al., 2014), representing high purity of the natural prepared pyrite. Two narrow peaks attributed at 2θ of 38.73 and 41.63 associated with the (2 1 0) and (2 1 1) planes confirm the prevailing presence of FeS_2 in the pyrite particles structures (Chen et al., 2018; Labiadh et al., 2015). Other considerable peaks positioned at 2θ of 28.15, 47.8, 58.1 and 63.7 are in accordance with the (1 1 1), (2 2 0), (2 2 2) and (2 3 0) planes, respectively, which also shows similarity between the pyrite exploited in this study and those derived from the natural material (Diao et al., 2017; Khataee et al., 2016). The FTIR spectra of raw pyrite and pyrite after four successive catalytic reaction cycles were determined to confirm the presence of surface functional groups (Fig.S2). Some distinguished peaks in the wavenumber range from 400 to 4000 cm^{-1} were detected. A moderate broad absorbance bond at 3432 cm^{-1} is related to the stretching hydroxyl group (Yang et al., 2019). Presence of a narrow band at 1640 cm^{-1} is attributed to C = C stretching vibration. The presence of typical peaks at 601 and 555 cm^{-1} were ascribed to the stretching vibration of the Fe–S band and asymmetric stretching vibration of Fe–O–OH species (Khataee et al., 2017). Although the bond at 407 cm^{-1} was confirmed in the standard pyrite FTIR (Sun et al., 2017), in this study it moved to a higher wavenumber of 478 cm^{-1} due to presence of some minor impurity including Cu, Al, and Si elements.

As pyrite has a natural origin, it is necessary to measure the primary elements existing in its structure. The elemental analysis of the pyrite particles, measured with the EDAX analyzer, is shown in Fig. S3. Fig. S3 shows that S and Fe were the primary elements found in the pyrite particles with weight percentages of 52.59% and 44.37%, respectively. Therefore, S and Fe are the operative parts that are contributing to the oxidation reactions. Moreover, the chemical composition of pyrite was analyzed with the XRF technique and related results are presented in Table S2. SO_3 (66.93%) and Fe_2O_3 (28.57%) were the main compounds present in the pyrite, confirming the EDAX results.

The surface morphology of pyrite was visualized by SEM micrography (Fig. S4a). The SEM image indicates that pyrite shaped from irregular and cubic particles. As is obvious from the SEM image, the pyrite cannot be considered as a porous material. Moreover, the BET technique showed that the specific surface area of the nanoparticles was only 11.614 m^2/g, confirming that the natural pyrite is a hardly porous material. On the other hand, the total pore volume of pyrite (at $P/P_0 = 0.981$) was calculated to be 6.339 cm^3/g along with the average pore size of 1.57 nm. It can be concluded that, based on IUPAC classification, the natural pyrite consists of mesoporous nanoparticles with a low specific surface area.

Fig. S4b shows a typical TEM image of pyrite particles. This image also confirms the cubic shape and non-homogeneous structure. The dark and bright areas of pyrite nanoparticles in Fig. S4b can be attributed to the pyrite particles with high and very thin density, respectively. The size distribution of pyrite nanoparticles induced from the TEM image is illustrated in Fig. S5 indicating that the particle size of most pyrite nanoparticles (nearly 80%) fall in the range of 30–70 nm. Moreover, the average particle size of pyrite was about 52.3 nm along with a standard deviation (SD) of 12.16 nm. Accordingly, it is specifically proved that the pyrite prepared from mine waste can be considered as a material formed from nanoparticles.

3.2. Effect of solution pH

To optimize the pH value, the influence of pH on the removal of TTC with the pyrite, sole H_2O_2 and pyrite/H_2O_2 processes was investigated, under experimental conditions presented in Table S1. The results are presented in Fig. 1. The effect of TTC hydrolysis and possible precipitation (due to various pK_a of 3.3, 7.7 and 9.7) was also evaluated, demonstrating no considerable decrease in initial TTC concentration at different pH values (lower than 1% of initial TTC concentration). As represented in Fig. 1, the maximum TTC adsorption by pyrite nanoparticles was only 8.3% at pH 8, and the change of solution pH values had no significant effect on TTC adsorption. Although some studies propose that pyrite alone has a high capability to remove emerging compounds such as sulasalazine (Khataee et al., 2017) and diclofenac (Bae et al., 2013), Fig. 1

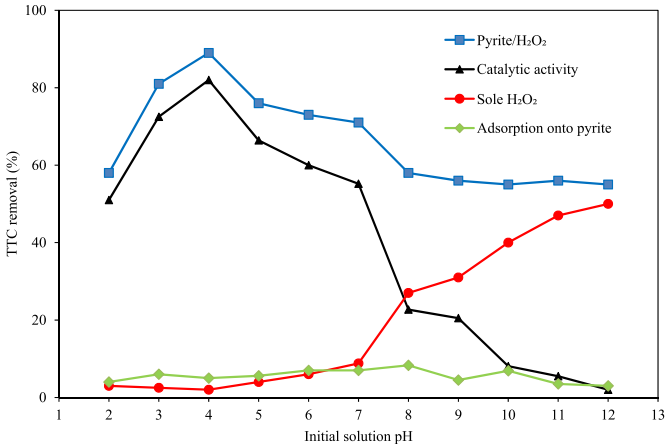

Fig. 1. Effect of initial solution pH on TTC removal in the sole H_2O_2, adsorption onto pyrite and pyrite/H_2O_2 processes (Reaction conditions: TTC concentration: 50 mg/L, pyrite concentration: 1 g/L, H_2O_2 concentration: 5 mmol/L, reaction time: 30 min).

shows that pyrite alone is not an efficient adsorbent for removal of TTC. Diao et al. (2017) discovered that the maximum removal of Rhodamine B compound with sole pyrite was only 15.7% at an initial Rhodamine B concentration of 19.6 mg/L and a pyrite dose of 1 g/L.

With increasing the solution pH value, the decomposition percentage of TTC increased in the sole H_2O_2 process. As revealed in Fig. 1, by the enhancement of pH from 2 to 7, the removal percentage of TTC slowly enhanced from 2% to 8.8%. Further increase of the pH value to 8 and then 12 resulted in a sharp enhancement of TTC degradation to 27% and 50%, respectively. From these findings, it was concluded that the sole H_2O_2 process was more efficient under alkalinity conditions than under acidic and neutral conditions. This phenomenon might be rationalzed by the physicochemical properties of TTC at different solution pH values (López-Peñalver et al., 2010). TTC molecules are amphoteric organic compounds containing one basic and two acidic functional groups (dimethyl amine, tricarbonyl amide and phenolic diketine, respectivly) which will appear in different ways as a function of pH. At pH lower than 3.3 (pKa1), most TTC molecules are comprehensively protonated and exist as $TTCH_3^+$; at 3.3 < pH < 7.7 (pKa 2), TTC molecules are present as $TTCH_2^0$; at 7.7 < pH < 9.7 (pKa3), the mojarity of TTC molecules are $TTCH^-$, and at pH value higher than 9.7 (pKa4), the TTC molesules exist dominantly as $TTCH^{2-}$ (Hopkins and Blaney, 2014). In a study conducted by Chen et al. (2017), the removal efficiency of TTC with sole H_2O_2 has been reported at different pH values. The results of this study demonstrated that with increase of pH, especially in alkaline solutions, the decomposition of TTC increased, corresponding to higher electron density in the ring structure of TTC^- and TTC^{2-} than TTC^+. Under these conditions, the attack of H_2O_2 and radical species will be promoted. Therefore, by the increase of solution pH, the degree of the TTC deprotonation is higher, and thus the removal rate increased accordingly.

Fig. 1 also showes that the maximum removal of TTC and catalytic activity were achieved at the acidic solution pH of 4, which respectively were 89% and 82%. For the pyrite/H_2O_2 process, the increase of pH from 4 to 12 lead to a decrease of TTC degradation from 89% to 55%, respectively. According to the above findings, the maximum TTC degradation and synergistic effect in the pyrite/H_2O_2 process was achieved at a pH of 4 which is close to the natural solution pH of TTC (appr. 4.1). At this pH, TTC is often found in its molecular shape so it could have a better reaction with $^{\bullet}OH$ present in the reactor (Yaghmaeian et al., 2017). Moreover, the pH of point of zero charge (pHpzc) of the pyrite nanoparticles in our study was determined to be 4.6 (Fig. S6). The pyrite surface was negatively charged at solution pHs above pHpzc and positively charged at solution pHs below pHpzc (Moussavi et al., 2012). Therefore, it could be expected that the surface of pyrite covered broadly with the hydroxyl groups (OH^-) at solution pHs of 4.6–12. As mentioned earlier, in the Fenton-like process, H_2O_2 reacts with the Fe^{2+} and finally OH^- and $^{\bullet}OH$ were generated as products (Eq. (1)). As the surface of pyrite shows a strong hydroxylation at pHs above pHpzc, especially under alkaline conditions, the reaction rate constant of $^{\bullet}OH$ production would be decreased due to accumulation of OH^- species on the pyrite surface and hinder the formation of Eq. (1). The reported values of pHpzc for pyrite in the literature ranged from 3.5 to 7.2 (Borah and Senapati, 2006; Bose et al., 2009; Duan et al., 2016), which can be related to the concentration of pyrite powder in solution, chemical composition of pyrite, degree of impurities, degree of temperature and hydration of pyrite formation and nature of crystallinity (Borah and Senapati, 2006; Oral and Kantar, 2019).

Therefore, a pH of 4.1 was considered as the optimum pH for the further experimental runs. From an operational standpoint, the fact that the maximum TTC removal attained at a natural TTC pH solution is an advantage, as it avoids the need to change acidity and/or alkalinity to adjust the pH of TTC solutions for achieving the desirable conditions.

3.3. Degradation mechanism

The maximum TTC degradation in the pyrite/H_2O_2 system may be due to the higher formation of $^{\bullet}OH$ as the main reactive oxygen species at acidic pH, which is agreed by many researchers (Cohn et al., 2006; Pham et al., 2008; Schoonen et al., 2010). However, a clear mechanism is missing. In general, production of $^{\bullet}OH$ and other oxide species in the aerobic pyrite slurries for TTC degradation may occur in three main ways as illustrated in Fig. 2. (i): without H_2O_2 addition, Fe (II) reacts with the O_2 (as an initiator) on

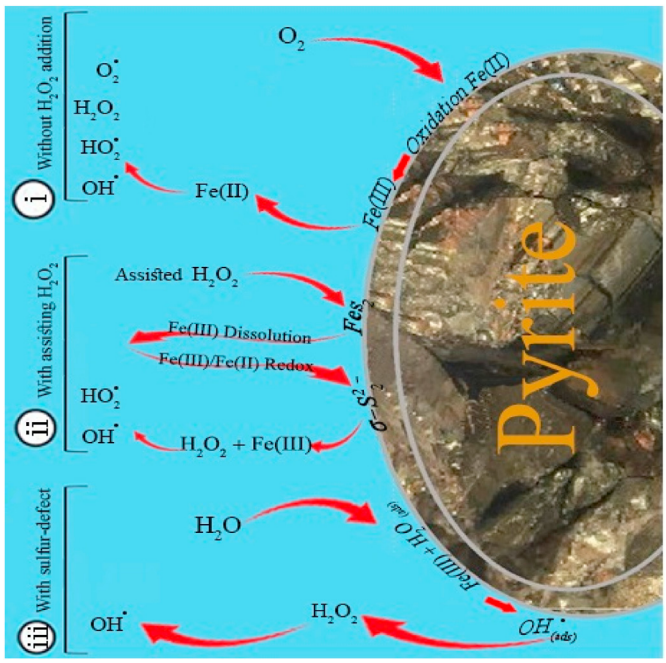

Fig. 2. Proposed pathways for $OH^{\bullet}$ production and other oxides species in pyrite slurries.

the surface of pyrite and is slowly oxidized to form Fe (III) and, then, continuous generation of Fe (II) on the pyrite surface leads to formation of $(O_2^{\bullet})^-$, H_2O_2, $HO_2^{\bullet}$ and $^{\bullet}OH$ (Che et al., 2011). (ii): With assistingH_2O_2, the pyrite-Fenton reaction may take place in the solution with attacking of H_2O_2 on the surface of the pyrite, leading to dissolution of Fe (III) according to Eq (5). The released Fe (III) can re-oxidize the pyrite surface with the strongly σ-binding reaction via pyrite disulfide (S_2^{2-}) group leading to generation of Fe (II) into solution (Eq. (6)). The released Fe (II) is oxidized to Fe (III) by some consecutive reactions with H_2O_2 to produce $HO_2^{\bullet}$ and $^{\bullet}OH$ (Eqs. (7) and (8)).

$$2FeS_2 + 15H_2O_2 \rightarrow 2Fe^{3+} + 4SO_4^{2-} + 2H^+ + 14H_2O \quad (5)$$

$$FeS_2 + 14Fe^{3+} + 8H_2O \rightarrow 15Fe^{2+} + 2SO_4^{2-} + 16H^+ \quad (6)$$

$$Fe^{2+} + H_2O_2 \rightarrow Fe^{3+} + OH^- + {}^{\bullet}O\,H \quad (7)$$

$$Fe^{3+} + H_2O_2 \rightarrow Fe^{2+} + HO_2^{\bullet} + H^+ \quad (8)$$

The H_2O_2 assisting mechanism and the above proposed reactions have well been studied and confirmed by numerous researchers (Che et al., 2011; Kantar et al, 2015b, 2019c; Oral and Kantar, 2019). (iii): With surface sulfur-defects, the interaction between adsorbed H_2O ($H_2O_{(ad)}$) and Fe^{3+} at a sulfur-deficient site on the surface of pyrite generates adsorbed $^{\bullet}OH$ ($^{\bullet}OH_{(ad)}$) (Borda et al., 2003; Chandra and Gerson, 2010; Zhang et al., 2016).

In order to specify the relative role of $^{\bullet}OH$ in the TTC degradation using pyrite/H_2O_2, catalytic processes in the presence of different radical scavengers and inhibitors including methanol, *tert*-butanol, salicylic acid, phosphate, chloride, sulfate, carbonate and bicarbonate were conducted. Fig. 3 shows the efficiency of TTC degradation with the pyrite/H_2O_2 process in the presence and absence of these radical scavengers. As indicated in Fig. 3, the degradation of TTC in the absence of scavengers was 88.5%, at a reaction time of 30 min, a pyrite dosage of 1 g/L, an initial TTC concentration of 50 mg/L, a H_2O_2 concentration of 5 mmol/L, and a pH of 4.1. Presence of scavengers including *tert*-butanol (TB), methanol (MT) and salicylic acid (SA) reduced the TTC degradation to 74.1, 66.4 and 12.5%, respectively. Based on the literature, TB and MT are the commonly used $^{\bullet}OH$ scavengers (Moussavi et al., 2018b). However, the reduction of decomposition in the presence of these two alcoholic scavengers is not outstanding. The reaction rate constant

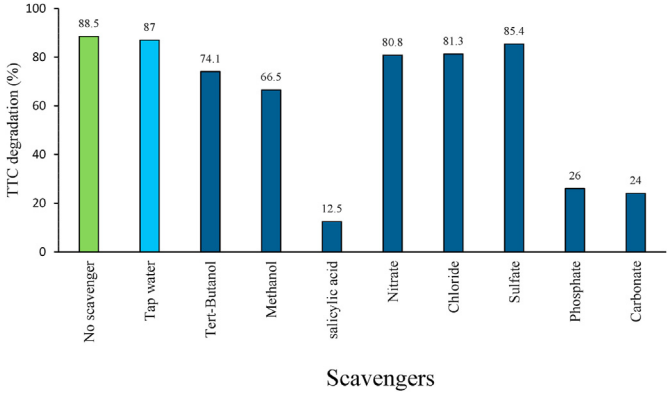

Fig. 3. TTC degradation efficiency in the pyrite/H_2O_2 process at presence of selected radical scavengers (reaction conditions: pH: 4.1, TTC concentration: 50 mg/L, pyrite dose: 1 g/L, reaction time: 30 min, H_2O_2 concentration: 5 mmol/L. The concentration of radical scavengers/inhibitors was 0.5 mmol/L except salicylic acid (0.1 g/L)).

of TTC with $^{\bullet}OH$ is 7.7×10^9 M^{-1} s^{-1} (Wols and Hofman-Caris, 2012), while in the presence of the TB and MT the reaction rate constants are 6×10^8 M^{-1} s^{-1} and 9×10^8 M^{-1} s^{-1}, respectively (Moussavi et al, 2016, 2018a). That is why another $^{\bullet}OH$ scavenger was used for proving the $^{\bullet}OH$ generation. The reaction rate constant of SA by $OH^{\bullet}$ has been reported to be 2.2×10^{10} M^{-1} s^{-1} (Moussavi et al., 2018b). So, the considerable reduction of TTC degradation in the presence of SA as a super $^{\bullet}OH$ scavenger emphasis that $^{\bullet}OH$ has been the main oxidizing agent.

Regarding the radical scavengers and inhibitor tests, it can be concluded that $^{\bullet}OH$ is the main reactive oxygen species that participate in the decomposition of TTC molecules. Meanwhile, additional experiments were conducted to better clarify the $^{\bullet}OH$ propagation for each proposed mechanism and TTC degradation in the pyrite-Fenton process.

In order to evaluate the role of molecular O_2 reduction and reaction with Fe^{2+} (mechanism (i)), the degradation of 50 mg/L of TTC with 1 g/L of pyrite at a retention time of 30 min with a H_2O_2 concentration of 5 mmol/L was compared under pure O_2 bubbled and N_2 saturated conditions. As can be observed from Fig. S7, TTC degradation was still above 85% implying that no considerable (below 4%) loss of TTC degradation efficiency takes place in both presence and absence of oxygen. Therefore, it can be concluded that dissolved oxygen did not considerably contribute to the generation of $^{\bullet}OH$ radicals. To evaluate the contribution of dissolved O_2 reduction to $^{\bullet}OH$ formation, similar experiments under various concentrations of Fe^{3+} (0.5, 1, 2 and 3 mmol/L) were also conducted. Fe^{3+} was chosen as an O_2 scavenger, as the reaction rate of Fe^{3+} with O_2 is an order of magnitude larger than that of pyrite nanoparticles (Chandra and Gerson, 2010; Hou et al., 2016). The quenching yields of various concentration of Fe^{3+} on O_2 reduction is shown in Fig. S8 as a function of TTC degradation. As observed from Fig. S8, the degradation of TTC slightly decreased from 88.5% to 85.7% with addition of Fe^{3+} from 0.5 mmol/L to 3 mmol/L, respectively, explaining that dissolved O_2 does not play an important role for $^{\bullet}OH$ generation.

As the degradation via $^{\bullet}OH$ radicals produced in the solution phase (mechanism (ii)) is inevitable and has well been established in the pyrite-Fenton process by many researchers (Che et al., 2011; Kantar et al, 2015a, 2015b, 2019a, 2019b, 2019c; Oral et al., 2017; Oral and Kantar, 2019; Rahim Pouran et al., 2014; Shaida et al., 2018), additional experimental runs to prove the incidence of this reaction doesn't seem necessary. Moreover, the total concentration of Fe in the treated TTC solution at present work was measured and detected to be about 0.43 mg/L, which confirmed the occurrence of the pyrite-Fenton reaction to produce solution phase $^{\bullet}OH$ radicals.

In order to evaluate the role of surface sulfur-defects reaction (mechanism (iii)) for probable $^{\bullet}OH$ generation, some specific tests were conducted. As can be observed from Fig. 3, presence of phosphate and carbonate lead to a reduction of TTC degradation efficiency to 26% and 24%, respectively. As phosphate and carbonate are hard-bases anions, they have high affinity to the Lewis acids and therefore can occupy the active sites of the pyrite surface (Mashayekh-Salehi et al., 2017), causing a loss of TTC degradation efficiency. They block the H_2O and H_2O_2 attack on the pyrite surface, leading to failed pyrite-Fenton and surface sulfur-defects reactions for generation of $^{\bullet}OH$ radicals. Meanwhile, experiments suggest that $^{\bullet}OH$ could be produced on the catalyst surface. In order to gain more experimental proof on the role of surface sulfur-defects in generation of $^{\bullet}OH$ radicals an optical and photoluminescence (PL) analysis was used at room temperature and the results are shown in Fig. 4. It is well known that defect states generated by the sulfur create additional levels and electronic transitions (Kharangarh et al., 2018). In the PL spectrum, emission spectrum and quantum yield of samples were examined with PL by

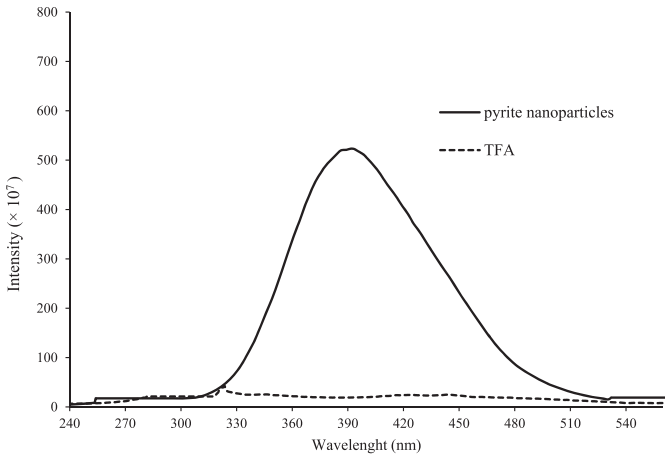

Fig. 4. The results of photoluminescence tests using TFA solution and pyrite nanoparticles.

recording at various excitation wavelengths from 240 nm to 540 nm with an interval of 40 nm (Charbouillot et al., 2011). Kharangarh et al. (2018) declared that defect states generated by the sulfur produce additional electronic transitions and energy levels. As indicated in Fig. 4, there is no clear peak in the solution with only TFA. On the other hand, a moderate intensity peak was obtained at wavelengths between 370 nm and 410 nm (with a peak at near 392 nm) from a sample containing pyrite, suggesting the presence of sulfur defects on the surface of the catalyst. The energy level obtained at 392 nm (~3.2 eV) obviously revealed the presence of sulfur related defects on the pyrite surface (Hochi et al., 2016; Kharangarh et al., 2018).

These experimental runs show that the following mechanisms may also involve the radical formation in the pyrite/H_2O_2 process: $^{\bullet}OH$ is generated on the surface of pyrite because of the existence of sulfur-deficient sites, then a huge rate of $^{\bullet}OH_{(ads)}$ transform to $H_2O_{2(ads)}$ which desorb to the bulk solution leading to $^{\bullet}OH$ generation through Fenton mechanism. Dosing of additional H_2O_2 (5 mmol/L) can accelerate the proposed mechanism. A small ratio of the adsorbed $^{\bullet}OH$ straightly desorbs into the bulk solution:

$$FeS_2^{\bullet S} + H_2O \rightarrow FeS_2^{\bullet S-H_2O} \quad (9)$$

$$FeS_2^{\bullet S-H_2O} + \equiv FeS_2 \rightarrow FeS_2^{-\bullet OH} + H_2O \quad (10)$$

$$FeS_2^{-\bullet OH} + H_2O \rightarrow FeS_2 + {}^{\cdot}O\,H + H_2O \quad (11)$$

$$FeS_2^{-\bullet OH} + H_2O_2 \rightarrow FeS_2 + H_2O + {}^{\cdot}O\,H \quad (12)$$

The suffix $^{\bullet}S$ in the FeS_2 demonstrates the sulfur-defect sites on the pyrite surface that were accessible for interaction with H_2O.

Accordingly, it can be deduced that surface sulfur-defects interaction could participate in $^{\bullet}OH$ generation along with main solution phase $^{\bullet}OH$ propagation (interaction of H_2O_2 with leached Fe (II)) for the degradation of TTC molecules.

3.4. Effect of water matrix

For applicability prospects, TTC degradation was measured in the presence of common water anions such as nitrate, chloride, sulfate (0.5 mmol/L) and even in tap water. As shown in Fig. 3, degradation of TTC was not considerably affected in the presence of these anions, and degradation varied from 85% to 80%. Tap water, which contained almost all anions, did not affect the TTC degradation either, and 87.1% removal efficiency was reached in tap water. Therefore, it can be concluded that the pyrite/H_2O_2 process could be an effective process for TTC degradation even in complex matrixes. Wang et al. (Wang and Wang, 2018) and Liang and Su (2009) found in their studies that the rate constants of nitrate, chloride and sulfate interactions with $^{\bullet}OH$ are 4.8×10^9 M^{-1} s^{-1}, 4.3×10^9 M^{-1} s^{-1} and 1×10^6 M^{-1} s^{-1}, respectively. Nevertheless, TTC reacts with $^{\bullet}OH$ at a high rate constant causing high removal efficiencies, even in a complex matrix.

3.5. Effect of assisted H_2O_2 concentration and pyrite dosage in the pyrite/H_2O_2 process

It is well known that the initial concentration of H_2O_2 and the catalyst dosage directly influence the production of powerful radicals such as $^{\bullet}OH$ in the heterogeneous Fenton and Fenton-like processes (Bae et al., 2013; Chen et al., 2017; Cohn et al., 2006). Hence, evaluation of the H_2O_2 concentration and catalyst dose on TTC removal was performed under the conditions described in Table S1. As shown in Fig. 5a, in the sole H_2O_2 process, the TTC removal increased slowly from 3.3% to 25.3% when the initial H_2O_2 concentration was increased from 1 to 60 mmol/L. The smooth decomposition of TTC in this process was accomplished by only direct reaction of TTC and H_2O_2 molecules as an oxidizing agent. Some researchers have also observed a similar trend for sole H_2O_2 in TTC degradation and proposed that direct oxidation might be the main mechanism involved in the TTC degradation by sole H_2O_2 (Chen et al., 2017). However, in the pyrite/H_2O_2 process, the removal of TTC enhanced sharply from 54% to 88.4% with increasing

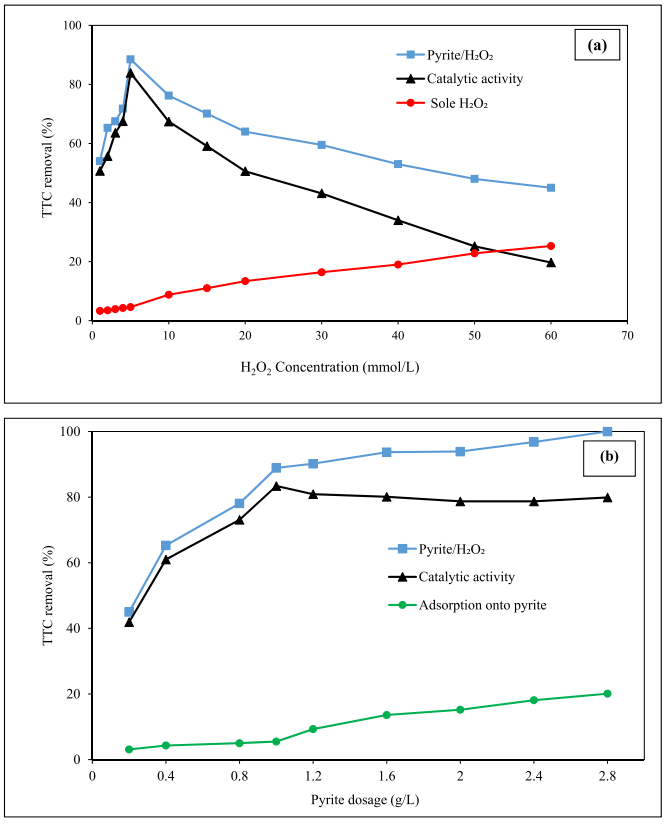

Fig. 5. Effect of (a) initial H_2O_2 concentration and (b) pyrite dosage on TTC removal in the sole H_2O_2 and pyrite/H_2O_2 processes (pH: 4.1, TTC concentration: 50 mg/L, reaction time: 30 min, pyrite dosage in (a): 1 g/L, and H_2O_2 concentration in (b): 5 mmol/L).

H_2O_2 concentration from 1 mmol/L to 5 mmol/L. Increase in TTC degradation with increasing H_2O_2 concentration in the pyrite/H_2O_2 process was closely related to the amount of Fe dissolved from pyrite surface and higher •OH production according to Eq. (5)- (8). Similar results were achieved by numerous researchers. Oral and Kantar (2019), for instance, observed in a study that diclofenac degradation increased with increasing H_2O_2 concentration in the pyrite-Fenton system. They found that a higher H_2O_2 concentration caused a higher attack on pyrite surface and more Fe dissolution leading to more formation of solution phase •OH.

Further increase of the initial H_2O_2 concentration to 60 mmol/L in the pyrite/H_2O_2 process caused a considerable reduction of TTC removal to 45%. The reduction of TTC removal with increase of H_2O_2 from 5 to 60 mmol/L can be related to the competitive reactions between H_2O_2 and •OH. It has been proven that H_2O_2 acts as both scavenger and promoter of •OH (Loeb, 2009). In excess of H_2O_2, it scavenges and transforms the •OH to form $HO^{\bullet}_2$ (hydroperoxyl radical), which has a lower oxidation capacity for TTC degradation in comparison with •OH, as shown in Eqs. (13) and (14) (Sharma et al., 2015).

$$H_2O_2\ (aq) + OH^{\cdot}O\ H \rightarrow\ HO^{\bullet}_2\ +\ H_2O \quad k =\ 2.7\ \times 10^{7}\ M^{-1}\ s^{-1} \tag{13}$$

$$HO^{\bullet}_2\ +\ ^{\cdot}O\ H \rightarrow O_2\ +\ H_2O \quad k =\ 6.6\ \times 10^{9}\ M^{-1}\ s^{-1} \tag{14}$$

Another reason for low removal rates of TTC with an increased H_2O_2 concentration in the pyrite/H_2O_2 process is the recombination of enhanced •OH to form H_2O_2 (Eq. (15)) (Imoberdorf and Mohseni, 2011; Sharma et al., 2015).

$$^{\cdot}O\ H + {}^{\cdot}O\ H \rightarrow H_2O_2 \quad k =\ 4.0\ \times 10^{9}\ M^{-1}\ s^{-1} \tag{15}$$

It has also been reported that the type and concentration of the pollutant, as well as reaction conditions are determining factors in the optimum initial concentration of H_2O_2 (Mirzaei et al., 2017). Although there is no similar study using the pyrite/H_2O_2 process for removal of TTC, some researchers have reported similar effects for H_2O_2 in heterogeneous Fenton-like processes for treating different organic compounds, using different experimental conditions (Giri and Golder, 2014; Mackulak et al., 2015). Because the maximum TTC removal and catalytic activity was attained at an initial H_2O_2 concentration of 5 mmol/L, the next pyrite/H_2O_2 experiments were conducted using 5 mmol/L of H_2O_2.

The influence of pyrite dosage on the TTC removal was also assessed. As presented in Fig. 5b, increase of the catalyst dosage from 0.2 g/L to 2.8 g/L, enhanced the TTC adsorption onto pyrite slightly from 3.1% to 20.1%, respectively. As mentioned before, maximum removal of TTC in the absence of pyrite (sole H_2O_2) was only about 4.6% under the applied experimental conditions. As illustrated in Fig. 5b, the TTC removal significantly increased to 88.9% in the presence of 1 g/L pyrite powder, implying a considerable catalytic role of pyrite at this concentration in the pyrite/H_2O_2 process. Thereafter, the removal of TTC gradually enhanced from 88.9% to 100% with an increasing pyrite dosage from 1 g/L to 2.8 g/L. The higher TTC degradation with increasing pyrite loading is due to the fact that the amount of Fe dissolved from pyrite also increases, leading to the generation of more •OH in solution, based on Eq. (7). A similar trend was observed in the study conducted by Kantar et al. (2019c) in the pyrite-Fenton process for chlorophenolic compounds degradation. They described that the reaction kinetics for degradation of chlorophenolic compounds are highly dependent on pyrite dose and, as pyrite loading increased from 0.25 to 1 g/L, the rate constants increased considerably due to higher generation of Fe (II) from reduction of Fe (III) on the increased pyrite surface. Labiadh et al. (2015) reported that the oxidation rate of AHPS dye improved along with initial pyrite concentrations in the heterogeneous electro-Fenton reactions. In another research performed by Khataee et al. (2017), it was reported that addition of 0.5 g/L pyrite powder to a sulfasalazine solution in a sono-catalytic reactor lead to about 98% sulfasalazine degradation during a contact time of 30 min. However, the optimum dosage of the catalysts in the catalytic processes is highly associated with the nature and concentration of the reactant and reaction conditions.

3.6. Influence of solution temperature and initial TTC concentration

The influence of various solution temperatures (15, 25 and 40 °C), as an important environmental factor, at different TTC concentrations was investigated for the pyrite/H_2O_2 process under selected conditions given in Table S1. In order to reach the equilibrium condition, a reaction time of 120 min was applied.

The results in terms of TTC removal as a function of initial concentration and solution temperature are presented in Fig. 6. As shown in the figure, both temperature and initial TTC concentrations affected the overall performance of the process. It was found that an enhancement of solution temperature from 15 °C to 40 °C leads to a TTC removal increase of about 14% (e.g. at 500 mg/L of initial TTC concentration). As shown in Fig. 6, the degradation efficiency enhanced with an increase of temperature for all given TTC concentrations. For instance, at reaction temperatures of 15, 25 and 40 °C, TTC removal efficiencies were 74%, 82.2% and 86.4%, respectively, at an initial concentration of 100 mg/L. Based on Arrhenius law, by increasing the solution temperature the •OH formation rate will be increased, but it also acts as a promoter for H_2O_2 degradation into oxygen and water molecules (Velichkova et al., 2013). Moreover, in solutions with a higher temperature the diffusion coefficients and mass transfer increase due to lower liquid viscosity. So, the increase in TTC degradation with increasing solution temperature can be due to the increase of TTC diffusion rates and mass transfer along with the effective collision between the TTC molecules in the bulk solution and oxidative agents (Moussavi et al., 2018a). As a result, a higher temperature has a positive effect on the TTC removal in the pyrite/H_2O_2 process, suggesting that heat act as •OH promoter.

The TTC removal decreased with increasing initial TTC concentration. For instance, by increase of initial TTC concentration from 25 mg/L to 500 mg/L at a solution temperature of 25 °C, the TTC removal decreased from 91% to 44%. Similar findings were reported

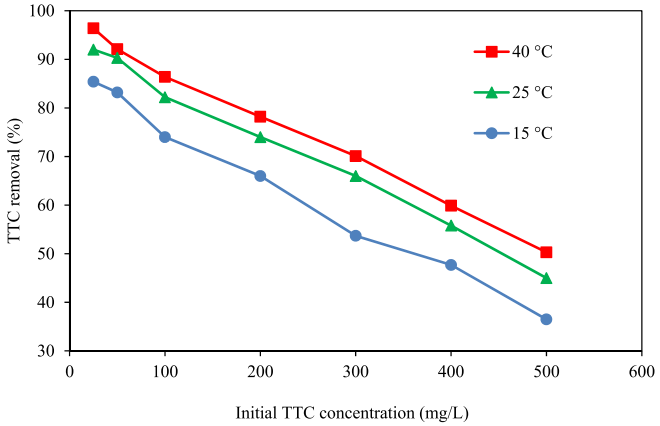

Fig. 6. Effect of solution temperature on TTC removal at different initial TTC concentration at pyrite/H_2O_2 process (Reaction conditions: pH: 4.1, H_2O_2 concentration: 5 mmol/L, pyrite dosage: 1 g/L, reaction time: 120 min).

in another study for TTC degradation (Hou et al., 2012), and for other pharmaceutical compounds including sulfasalazine (Khataee et al., 2017; Zou et al., 2014) and ofloxacin (Titouhi and Belgaied, 2016) using heterogeneous Fenton-like processes. In the pyrite/H_2O_2 process, the following parameters can hinder the removal of TTC at higher initial TTC concentrations under the same given conditions:

- The higher the amount of TTC molecules in the solution, the higher the reaction of dosed H_2O_2 with TTC molecules in the solution instead of interaction with surface of pyrite for the propagation of $^{\bullet}OH$.
- The higher TTC concentration in the solution may occupy a further amount of pyrite surface, preventing the generation of the reactive oxidants.
- Considering the constant generation of oxidizing agents in the process at constant situations, the ratio of oxidizing agents to the TTC molecules decreases resulting in the reduction of removal percentage.
- The by-products which were generated during the catalytic reaction may lead to side reactions, which may cause the competition between the main organic matter and its degraded intermediates in reacting via $^{\bullet}OH$. Accordingly, a higher initial TTC concentration leads to higher by-product generation, and subsequently the main pollutant degradation will be retarded.

3.7. Kinetic analysis and catalytic activity of pyrite for TTC degradation

The potential of pyrite nanoparticles in the degradation and mineralization of TTC was evaluated in terms of catalytic activity under selected conditions as defined in Table S1. The removal of TTC in the sole H_2O_2 process and pyrite/H_2O_2 process, as well as the catalytic activity of pyrite as a function of contact time are illustrated in Fig. 7a. The adsorption of TTC onto pyrite dose not have a considerable contribution to the degradation of TTC (smaller than 5.5% at a contact time of 30 min). It is therefore considered that TTC was removed mainly in the pyrite/H_2O_2 process. As shown in Fig. 7a, the efficacy of sole H_2O_2 in the degradation of TTC was enhanced from 3.9% to 22% by increasing the contact time from 1 min to 60 min. In comparison, addition of pyrite in the pyrite/H_2O_2 process causes a significant improvement of the TTC degradation from 26.1% at a contact time of 1 min–89% at a contact time of 30 min. Increasing the reaction time to 60 min caused the comprehensive removal of TTC. Basically, the catalytic activity of pyrite on the pyrite/H_2O_2 process, computed based on (Eq. (3).S), enhanced from 22.2% to a maximum of 79.5%, with the increase of reaction time from 1 min to 30 min.

Fig. 7b represent the TOC reduction as a function of contact time. As shown in Fig. 7b, TOC removal with the sole H_2O_2 process was around 7.7% at the maximum tested contact time and the TOC reduction in the pyrite/H_2O_2 process increased from 7% at a reaction time of 1 min–67% at a reaction time of 30 min. As can be seen in Fig. 7b, a significantly higher TOC reduction was gained in the pyrite/H_2O_2 process in contrast to in the sole H_2O_2 process. The potential of pyrite nanoparticles for catalyzing the TTC mineralization in the pyrite/H_2O_2 process was about 62% at a reaction time

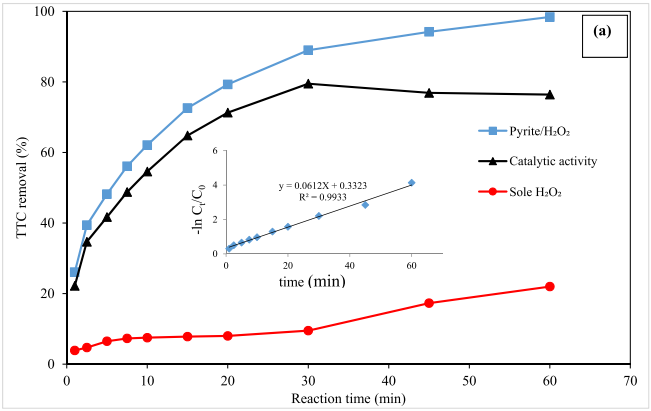

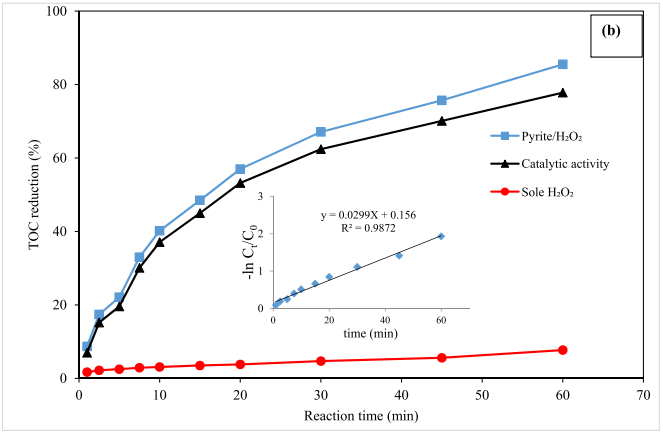

Fig. 7. Catalytic activity of pyrite for (a) TTC degradation and (b) TOC reduction in the pyrite/H_2O_2 process as a. function of contact time (pH: 4.1, H_2O_2 concentration: 5 mmol/L, pyrite dosage: 1 g/L, initial TTC concentration: 50 mg/L).

As COD is one of the most widely used indicators of the extent of organic compounds removal in various synthetic and real wastewater samples (Groele and Foster, 2019), the COD concentration of the TTC solution before and after treatment was also measured. It is known that significant levels of some inorganic species including manganese, ferrrous iron and sulfide cause inaccuracies in the COD analysis (Lee et al., 2011). Morover, it is well known that H_2O_2 interferes with the COD analysis by consuming oxidation agents such as $K_2Cr_2O_7$, thus leading to overestimation of the COD measurements (Raut-Jadhav et al., 2016). In this regards, the interference of iron and sulfide, as the main compounds present in the pyrite nanoparticles, and H_2O_2 on the COD concentration during the pyrite/H_2O_2 treatment process has been evaluated to obtain the true/corrected COD values. The true/corrected value of COD (mg/L) after treatment was calculated according to Eq. (16):

$$\text{True / Corrected COD} = \text{measured COD} - \text{extent of COD overestimation} \quad (16)$$

In order to evaluate COD overestimation, the concentration of COD in the pyrite/H_2O_2 suspension with distilled water (without TTC) was measured at the same conditions as used in the pyrite/H_2O_2 treatment process for TTC removal (pH: 4.1, H_2O_2

Table 1
Comparison of removal efficiency of water organic pollutants using non-waste natural pyrite prepared from mine as catalyst reported in literature.

Process	Shape and purification method	Pollutant(s)	Experimental conditions	Degradation efficiency	K_{obs} (min^{-1})	Fitted model	Correlation coefficient (R^2)	Ref.
Heterogeneous sono-Fenton	Nanorods, non-thermal plasma	Anthraquinone dye	• pH: 3-11 • Reaction time: 0 −40 min • Initial contaminant concentration: 20−50 mg/L • H_2O_2 concentration: 0 −2 mM • Power density: 0 −300 W/L • pyrite dosage: 0 −0.8 g/L • Temperature: not reported	100% @ 40 min	0.0594	PFO	0.985	(Khataee et al., 2016)
Heterogeneous sono-Fenton-Like	Nanostructured, Ar glow discharge plasma	Textile dye	• pH: 2-9 • Reaction time: 0 −120 min • Initial contaminant concentration: 10−40 mg/L • Ultrasonic power: 0 −300 W/L • pyrite loading: 0 −5 g/L • Temperature: ambient	93.7% @ 120 min	0.0205	PFO	0.994	(Khataee et al., 2016)
Pyrite/H_2O_2	Nanoparticles obtained from magnetite ore, no further purification	Acid orange 7	• pH: 2-9 • Reaction time: 5 −25 min • Initial contaminant concentration: 4 −20 mg/L • H_2O_2 concentration: 1 −5 mmol/L • Catalyst loading: 0.1−0.5 mg/L • Temperature: ambient	96.3% @ 25 min	Not reported	Not reported	0.989	(Fathinia et al., 2015)
• Pyrite/Potassium persulfate • Pyrite/H_2O_2	Microparticles supplied from sulfure-polymetallic, cleaned with 0.1 M HNO_3	Rhodamine B	• pH: 2-11 • Reaction time: 0 −120 min • Initial contaminant concentration: 19.6 mg/L • H_2O_2 concentration: 2 −10 mM • Pyrite loading: 1 g/L • Persulfate loading: 2 −10 mM • Temperature: 25 ± 1 °C	• 98% @ 120 min • 99% @ 120 min	• 0.0304 • 0.0392	• PFO • PFO	• 0.987 • 0.996	Diao et al. (2017)
Heterogeneous electro-Fenton	Microparticles. Ultrasonication in ethanol (95%) for 5 min, washed and then rinsed with 1 M HNO_3 and deionizedwater, respectively.	Sulfamethazine	• pH: 6.1 • Reaction time: 0 −480 min • Initial contaminant concentration: 0.2 mM • Current intensity: 100 −1000 mA	96% @ 30 min	0.061	PFO	0.988	(Barhoumi et al., 2016)

(*continued on next page*)

Table 1 (*continued*)

Process	Shape and purification method	Pollutant(s)	Experimental conditions	Degradation efficiency	K_{obs} (min^{-1})	Fitted model	Correlation coefficient (R^2)	Ref.
			• Pyrite loading: 0.5–4 g/L • Temperature: room					
Fenton oxidation	Microparticles, Ultrasonicate for 5 min in ethanol and washed by nitric acid (1 M)	Diclofenac	• pH: 3-6 • Reaction time: 0–400 s • Initial contaminant concentration: 0.017 mM • H_2O_2 concentration: 0.12–2.4 mM • Pyrite loading: 0.42–6.24 mM • Temperature: 25 ± 0.5 °C	100% @ 120 s	0.06–1.66 S^{-1}	PFO	0.985	Bae et al. (2013)
Sono-catalytic	Nanoparticles, crushing, gringing, milling and separating by magnetic separators	Sulfasalazine	• pH: 3-9 • Reaction time: 0–30 min • Initial contaminant concentration: 10–40 mg/L • Ultrasonic frequency: 40–60 kHz • Catalyst loading: 0.1–0.5 g/L • Temperature: room	97% @ 30 min	0.1128	PFO	0.98	Khataee et al. (2017)
Heterogeneous ozonation	Nanoparticles, Wet impregnation	Reactive Black 5	• pH: 3-10 • Reaction time: 0–120 min • Initial contaminant concentration: 200 mg/L • Ozone dosage: 5.6 mg/min Catalyst loading: 2.5 g/L • Temperature: room	~60% @ 120 min	Not reported	Not reported	Not reported	Wu et al. (2016)
Pyrite-Fenton	Microparticles, no further purification	Diclofenac sodium	• pH: 5.1 • Reaction time: 0–50 min • Initial contaminant concentration: 100 mg/L • H_2O_2 concentration: 0.005–0.3 • Pyrite dosage: 0.25–1 g/L • Temperature: 30 °C	100% @ 60 min	0.0203	First-order	0.95	Oral and Kantar (2019)
Pyrite/ peroxydisulfate	Nanoparticles, washing by ultrapure water	Acetaminophen	• pH: 4-10 • Reaction time: 0–360 min • Initial contaminant concentration: 50 mg/L • pyrite dosage: 2 g/L • Peroxydisulfate: 5 mM	96.6% @ 180 min	Not reported	Not reported	Not reported	(Peng et al., 2018)
Pyrite-Fenton process for degradation of	Microparticles, no further purification	• 2-CP • 4-CP • 2,3-DCP	• pH: 3-5 • Reaction time: 0–120 min	Complete TOC removal	• -0.1637 • -0.2411 • -0.2269	First-order	• 0.98 • 0.99 • 0.99	Kantar et al. (2019c)

Table 1 (*continued*)

Process	Shape and purification method	Pollutant(s)	Experimental conditions	Degradation efficiency	K_{obs} (min^{-1})	Fitted model	Correlation coefficient (R^2)	Ref.
various chlorophenolic compounds (CP)		• 2,4-DCP • 2,4,6-TCP • 2,3,4,6-TeCP	• Initial contaminant concentration: 100–200 mg/L • Pyrite dosage: 0.25–1 g/L • H_2O_2 concentration: 0.3 mM • Temperature: ambient	was not attained	• -0.1045 • -0.0721 • -0.3389		• 0.99 • 0.99 • 0.98	
Pyrite/Persulfate	Microparticles, rinsed with distilled water, 50% HCl and ethanol	Tris (2-chloroethyl) phosphate (TCEP)	• pH: 3-11 • Reaction time: 0–120 min • Initial contaminant concentration: 2 mg/L • Persulfate concentration: 0.5–5 mM • pyrite dosage: 0.03–0.5 g/L • Temperature: ambient	100% @ 120 min	$-(3.23 \pm 0.33) \times 10^{-2}$	PFO	0.9401	(Lian et al., 2019)
Fenton-type photocatalyst	Microparticles obtained from metallurgical slag (about 70% Fe_2O_3), stirred and centrifuged with water for 10 min at 500 rpm.	Diclofenac	• pH: 5-9 • Reaction time: 20–60 min • Initial contaminant concentration: 30–120 mg/L • H_2O_2 concentration: 1000–3000 mg/L • Catalyst dosage: 1000-300 mg/L • Irradiation: 250–750 W/m^2 • Temperature: 25 °C	100% @ 90 min	0.046	PFO	0.98	(Arzate-Salgado et al., 2016)
Sole pyrite	Miroparticles induced graphite mine, no further purification	Carbofuran	• pH: 2.5–5 • Reaction time: 0–300 h • Initial contaminant concentration: 5 μM • Pyrite dosage: 2.7–47 μM • Temperature: 25 °C	~40% @ 100 h	0.011 h^{-1}	PFO	Not reported	(Dhanasekara et al., 2015)
Sole pyrite	Microparticles derived S-polymetallic mines, no further purification	p-chloroaniline	• pH: 3-11 • Reaction time: 0–360 min • Initial contaminant concentration: 0.03 mM • Pyrite dosage: 4 g/L • Temperature: 20 °C	54.99% @ 350 min	Not reported	Not reported	Not reported	Zhang et al. (2015)
Pyrite/H_2O_2	Nanoparticles, Ultra-sonication	TTC	• pH: 2-12 • Reaction time: 1–60 min • Initial contaminant concentration: 25–500 mg/L	89% @ 30 min, 100% @ 60 min	0.0612 min^{-1}	PFO	>95%	Present work

(*continued on next page*)

Table 1 (*continued*)

Process	Shape and purification method	Pollutant(s)	Experimental conditions	Degradation efficiency	K_{obs} (min^{-1})	Fitted model	Correlation coefficient (R^2)	Ref.
			• Pyrite dosage: 0.2–2.4 g/L • H_2O_2 concentration: 0.5–60 mM • Temperature: 15 –40 °C					

concentration: 5 mmol/L, pyrite dosage: 1 g/L). The COD concentrations of the initial TTC solution, the TTC solution after pyrite/H_2O_2 process and the pyrite/H_2O_2 suspension with distilled water (without TTC) were 110 mg/L, 140 mg/L and 116 mg/L, respectively. Therefore, the corrected COD value of TTC after pyrite/H_2O_2 process was calculated as 24 mg/L (140-116 mg/L). This implied a COD reduction efficiency of 78%.

Many other previous reports have also confirmed the interference of H_2O_2 on the COD estimation (Kang et al., 1999; Kuo, 1992; Raut-Jadhav et al., 2016). Hydrogen peroxide leads to a COD overestimation since it gets consumed during COD analysis as shown in the oxidation reaction given in Eq. (17) (Talinli and Anderson, 1992), leading to more utilization of potassium dichromate and higher COD values.

$$K_2Cr_2O_7 + 3H_2O_2 + 4H_2SO_4 \rightarrow K_2SO_4 + Cr_2(SO_4)_3 + 7H_2O + 3O_2 \quad (17)$$

TTC degradation by TiO_2 photocatalysis was studied by Reyes et al. (2006). They reported that complete degradation of TTC was attained at a reaction time of 40 min. In contrast, 50% of COD and 20% of TOC was removed at the initial synthetic TTC solution of 7.3×10^{-2} mmol/L.

Degradation and mineralization kinetics were also investigated in the present study, based on the pseudo-first-order reaction model using the following equation (Moussavi et al., 2016; Pourakbar et al., 2016):

$$\ln\left(\frac{C_t}{C_0}\right) = -k_1 t \quad (18)$$

Where C_t and C_0 are the TTC and TOC concentration, respectively, in the solution before and after the experiment, and k_1 is the reaction rate constant of Pseudo First Order (PFO) model. The R^2 values (>0.95) presented in Fig. 7 show that the PFO kinetic model has a good fit with the experimental results of TTC degradation and TOC reduction in the pyrite/H_2O_2 process. As shown in Fig. 7, the reaction rate constant of the TTC degradation (0.0612 min^{-1}) is almost 2 times higher than that of TOC reduction (0.0299 min^{-1}). This difference in the reaction rate constants demonstrates that TTC molecules are oxidized in the first step with higher reaction rate, contributing to the generation of organic by-products. There is no similar study using pyrite for TTC degradation to enable direct comparison. However, the reaction rate constants in the pyrite/H_2O_2 process are comparable with other AOPs. For example, Qiao et al. (2019) applied a sonocatalytic process using a novel catalyst ($SrTiO_3/Ag_2S/CoWO_4$) for TTC degradation, the highest reaction rate constant (0.007 min^{-1}) value reported in this study was almost 9 times lower than the ones reported in the present study.

3.8. Comparison with pyrite from other origin as catalyst in the AOPs

The performance of other pyrite samples, non-waste mineral and synthetic ones, as catalyst for the removal of organic pollutants in aqueous solution, was compared with the present study and the results are presented in Table 1 and Table 2, respectively. The comparison of degradation efficiency and reaction time (column 5, Tabels 1 and 2) revealed that the used pyrite from mine waste has similar and/or better performance characteristics compared to non-waste mineral pyrite and synthetic pyrite, indicating that the waste mine pyrite is a promising effective catalyst in the Fenton-like process at aquouse solution.

3.9. Catalyst reusability and sustainability

The reusability and durability of the nano pyrite particles was evaluated during 4 cycles under repeated optimal identical conditions as defined in Table S1. For this aim, the used pyrite nanoparticles were filtered from the suspension solution, at the end of each cycle, washed, dried at 60 °C in a sealed quartz tube to prevent further oxidation in air, and then applied to the next cycle. The removal of TTC for these four successive cycles is presented in Fig. 8. As shown in Fig. 8, it was found that the TTC removal is still high after four successive cycles within a reaction time of 120 min in each cycle. The TTC removal for fresh pyrite nanoparticles was about 96.1%; and, after four consecutive cycles of reusing pyrite, the percentage of TTC removal was not considerably affected and stayed above 90%.

In addition, the concentration of leached total iron in solution at the end of each cycle was measured. The total released iron decreased gradually from 0.43, 0.32, 0.21 to 0.17 mg/L in the first to fourth cycle, respectively. Nevertheless, the TTC removal percentages were still high after four subsequent cycles. Moreover, the FTIR spectra and XRD patterns of used pyrite showed little variation in contrast to the raw pyrite nanoparticles. Diao et al. (2017) conducted a comparative study between pyrite/persulfate and pyrite/H_2O_2 process for rhodamine B degradation and reported that the prepared catalyst maintained its reusability after five experimental cycles in the systems. Actually, it can be concluded that pyrite nanoparticles in the present study are reusable catalysts with appropriate durability and high removal efficiencies.

3.10. Identification of inorganic and organic intermediates in the pyrite/H_2O_2 process

The fate of 50 mg/L of TTC was evaluated in the pyrite/H_2O_2 process at the reaction condition of pH: 4.1, H_2O_2 concentration: 5 mmol/L, pyrite dosage: 1 g/L and contact time: 60 min. The main inorganic generated intermediates of TTC removal in the pyrite/H_2O_2 process are due to the cleavage of C–N bonds which exist in the structure of TTC molecules. Since there are no other bonds such as C–S and C–Cl in the structure of TTC, aqueous N by-products are

Table 2
Comparison of removal efficiency of water organic pollutants using syntetisis pyrite originated from mine as catalyst reported in literature.

Process	Shape and preparation methods	Pollutant	Experimental conditions	Degradation efficiency	K_{obs} (min^{-1})	Fitted model	Correlation coefficient (R^2)	Ref.
•Pyrite/ peroxymonosulfate •Pyrite/peroxydisulfate • Pyrite/H_2O_2	Nanoparticles, Iron disulfide (95%)	1,4-dioxane	• pH: 3.5−10 • Reaction time: 0−60 min • Initial contaminant concentration: 50 mg/L • Peroxymono/disulfate: 0.5−2.3 mM • H_2O_2 concentration: 0.5 −2.3 mM • Catalyst loading: 0.5−5 g/L • Temperature: ambient	• ~100% @ 40 min • ~50% @ 40 min • ~15% @ 40 min	• 0.061 • 0.016 • 0.005	• PFO • PFO • PFO	• 0.979 • 0.958 • 0.973	(Feng et al., 2018)\
Visible light improved by Pyrite-Fenton	Solvethermal method with mixure of $FeSO_4.7H_2O$, $Na_2S_2O_3$ and S	p-nitrophenol	• pH: 2.5−6 • Reaction time: 0−60 min • Initial contaminant concentration: 25 −400 mg/L • H_2O_2 concentration: 2 −10 mM • FeS_2 loading: 0.1−0.6 g/L • Temperature: room	100% @ 10 min	0.0481	Not reported	0.9941	(Zeng et al., 2019)
Ultrasound-assisted heterogeneous Fenton-like	Microparticles, analytical Fe_3O_4	TTC	• pH: 3-7 • Reaction time: 0−60 min • Initial contaminant concentration: 100 mg/L • Catalyst dosage: 0.5−2 g/L • H_2O_2 concentration: 10 −250 Mm • Ultrasound power: 40 −90 W • Temperature: 10−60 °C	93.6% @ 60 min	Not reported	Not reported	Not reported	Hou et al. (2016)
Fenton-Like	Nanoparticles, $FeSO_4.7H_2O$ were mixed with $Na_2S_2O_3.5H_2O$	• Diclofenac	• pH: 2-10 • Reaction time: 0−3 min • Initial contaminant concentration: 10 −50 mg/L • Catalyst dosage: 0.02 −0.2 g/L • H_2O_2 concentration: no added • Temperature: ambient	100% @ 20 min in the natural pH	0.904 (S^{-1})	PFO	Not reported	(Khabbaz and Entezari, 2017)
Heterogeneous Fenton reagent- Fe_2GeS_4	Nanoparticles of Fe_2SiS_4, Fe, Si and S powders were mixed to the stoichiometric ratio of 2:1:4, respectively.	• Methylene blue • Rhodamine Methyl orange	• pH: 3-11 • Reaction time: 0−10 min • Initial contaminant concentration: 20 mg/L • Catalyst loading: 0.1−1 g/L • H_2O_2 concentration: 10 −90 mmol/L • Temperature: ambient	• 100% @ 5 min • 100% @ 5 min • 100% @ 10 min	Not reported	Not reported	Not reported	(Shi et al., 2018)
Heterogeneous Fenton	Fe_3O_4 nanoparticles, chemical coprecipitation of $FeCl_2.4H_2O$ and $FeCl_3.6H_2O$ in 100 mLdeoxygenated water.	Norfloxacin	• pH: 2.5−9.5 • Reaction time: 0−60 min • Initial contaminant concentration: 0 −100 mg/L • H_2O_2 concentration: 0 −49 mM • Catalyst loading: 0.1 −0.5 g/L • Temperature: 15−45 °C	100% @ 60 min	Not reported	Not reported	Not reported	(Niu et al., 2012)
Heterogeneous Photo-Fenton by visible light	Nanoparticles of Fe_2SiS_4, Fe, Si and S powders were mixed to the stoichiometric ratio of 2:1:4, respectively.	Methylene blue	• pH: 2-10 • Reaction time: 0−20 min • Initial contaminant concentration: 5 g/L • H_2O_2 concentration: 0.5 mM • Catalyst loading: 0.5 g/L• Temperature: not mentioned	96.9% @ 10 min	0.55957	PFO	0.98	(Shi et al., 2018)

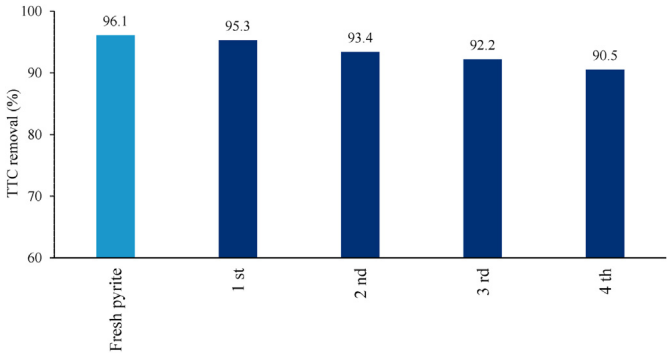

Fig. 8. The reusability and durability of pyrite for TTC degradation (pH: 4.1, H_2O_2 concentration: 5 mmol/L, pyrite dosage: 1 g/L, reaction time: 120 min).

the main inorganic intermediates which can be generated. Therefore, the concentration of aqueous N products including ammonium, nitrite and nitrate was monitored as a function of contact time (1–60 min). The results are presented in Fig. 9a. These inorganic intermediates are generated due to the detaching and converting of nitrogen atoms in the amide and amine groups of TTC molecules. The stoichiometric concentration of N atoms in the 50 mg/L TTC solution was calculated to be 3.15 mg N/L. As illustrated in Fig. 9a, nitrite was the main generated by-product at the earlier reaction times (3 mg N/L), but continuing the reaction leads to the reduction of nitrite to 0.07 mg N/L. Decreasing nitrite concentrations, along with decreasing total N concentration in the solution, proves that the nitrite is reduced in the pyrite/H_2O_2 process to gaseous nitrogen-containing by-products. Nevertheless, within the reaction time, the concentration of nitrate remains lower than 0.22 mg N/L. Moreover, the ammonium concentration increased from 0.03 to 0.3 mg N/L when the reaction time was enhanced from 1 to 15 min. Then, the concentration of ammonium had negligible fluctuations. Another observation from Fig. 9a is that the concentration of total nitrogen increased sharply from 0.8 to 3.1 mg-N/L when the contact time raised from 1 to 5 min. The stoichiometric (3.15 mg N/L) and measured (3.1 mg N/L) values of total nitrogen concentration at the retention time of 5 min, which are very close, suggest that the pyrite/H_2O_2 process is capable of completely cleaving the C–N bond in the TTC molecules within the initial stage. Thereafter, the total nitrogen concentration reduced to 0.3 mg N/L at the end of the experiment. Based on experimental results reported by Wu et al. (2012), inorganic ions including nitrate and ammonium can be formed by further oxidation of short-chain carboxylic acids by-products deduced from TTC molecules. Zhu et al. (2013) found that the ammonium ion was one of the end-products of TTC oxidation in the photocatalytic process. Regarding to the mass balance of total aqueous nitrogen, with a difference between the measured concentration of N at the beginning and at the end of the reaction, it may be concluded that most of the nitrogen existing in the TTC structure can be effectively changed to the less hazardous species in aqueous solution including nitrogen oxide gases such as NO_2, N_2O and N_2.

Due to the structural stability of the antibiotics, complete mineralization is not easily reached (Wolters and Steffens, 2005). Therefore, organic by-products were also followed in the present study using LC-MS analysis in positive and negative mode matching by [M + H^+] and [M-H^+], respectively, at m/z of 25–500. Fig. 9b shows the LC-MS chromatogram of the TTC and other detected by-products. It can be observed that no TTC spectrum (at 445 m/z) was recognized and the chromatogram mainly included short signal peaks representing that TTC degradation was effectively achieved under the selected condition. Table S3 lists the main intermediates

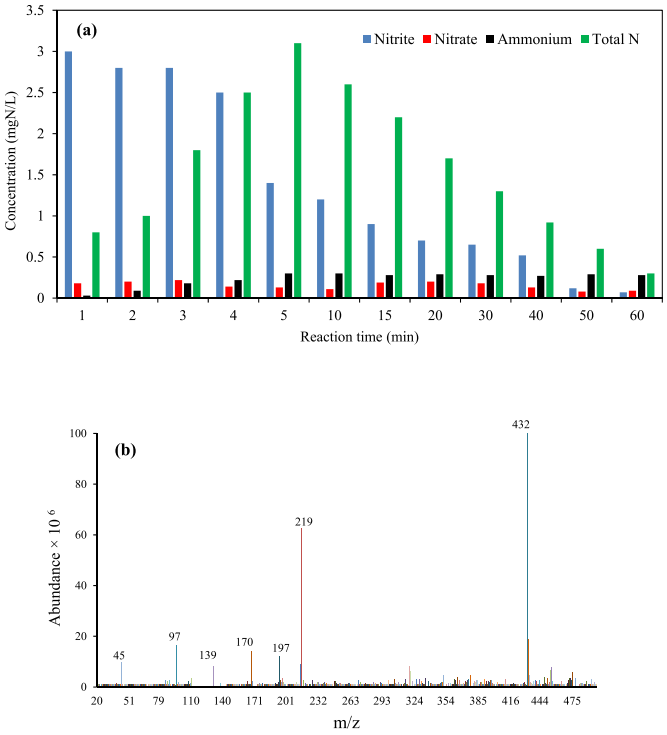

Fig. 9. Concentration of different inorganic intermediates (a) and the LC/MS chromatogram of the treated TTC solution (b).

detected in the treated solution along with their molecular structure and weight as well as m/z ion mode. As illustrated in Fig. 9b, the m/z of 432 and 219 fragmentation ions were the highly detected signals, which suggests that N-methyl groups are generated due to the low energy bond of C–N along with ring cleavage by hydroxyl radicals at the end of the degradation reaction (Zhu et al., 2013). Moreover, further oxidation with •OH of amine bonds and then benzene ring of TTC lead to the formation of small-chain carboxylic acids intermediates (Wu et al., 2012). Further oxidation reactions of organic intermediates by hydroxyl radicals caused to yield mineral products including nitrate, nitrite and ammonium.

3.11. Proposed pathways of TTC degradation in the pyrite/H_2O_2 system

According to the transformation products detected in the present study (inorganic and organic by-products) and previous studies (Ao et al., 2019; Jeong et al., 2010; Wang and Wang, 2018), one of the possible oxidation pathway is illustrated in Fig. 10. In summary, the pattern of TTC decomposition could be accomplished by the attack of hydroxyl radicals into three main pathways including conjugated phenolic groups, aromatic rings and double bounds that have relatively high electron density (Ao et al., 2019; Liu et al., 2018; Wang et al., 2018). Wang et al. (2018) found that dual bonds are the most probable groups to be attacked with •OH due to higher electron-rich properties. They found that the •OH attack was expected to happen by adding a –OH group (hydroxylation process at C11a position) to generate the primary by-products with the m/z of 461. Afterwards, it could be converted into other intermediates with the m/z of 458, 432 and 430 (not detected at the present LC/MS analyses) by further degradation via hydrogen abstraction, decarbonylation and demethylation, respectively. The H-abstraction at C5a via •OH attack on m/z = 461 could lead to production of m/z = 458 (Li and Hu, 2016). In the

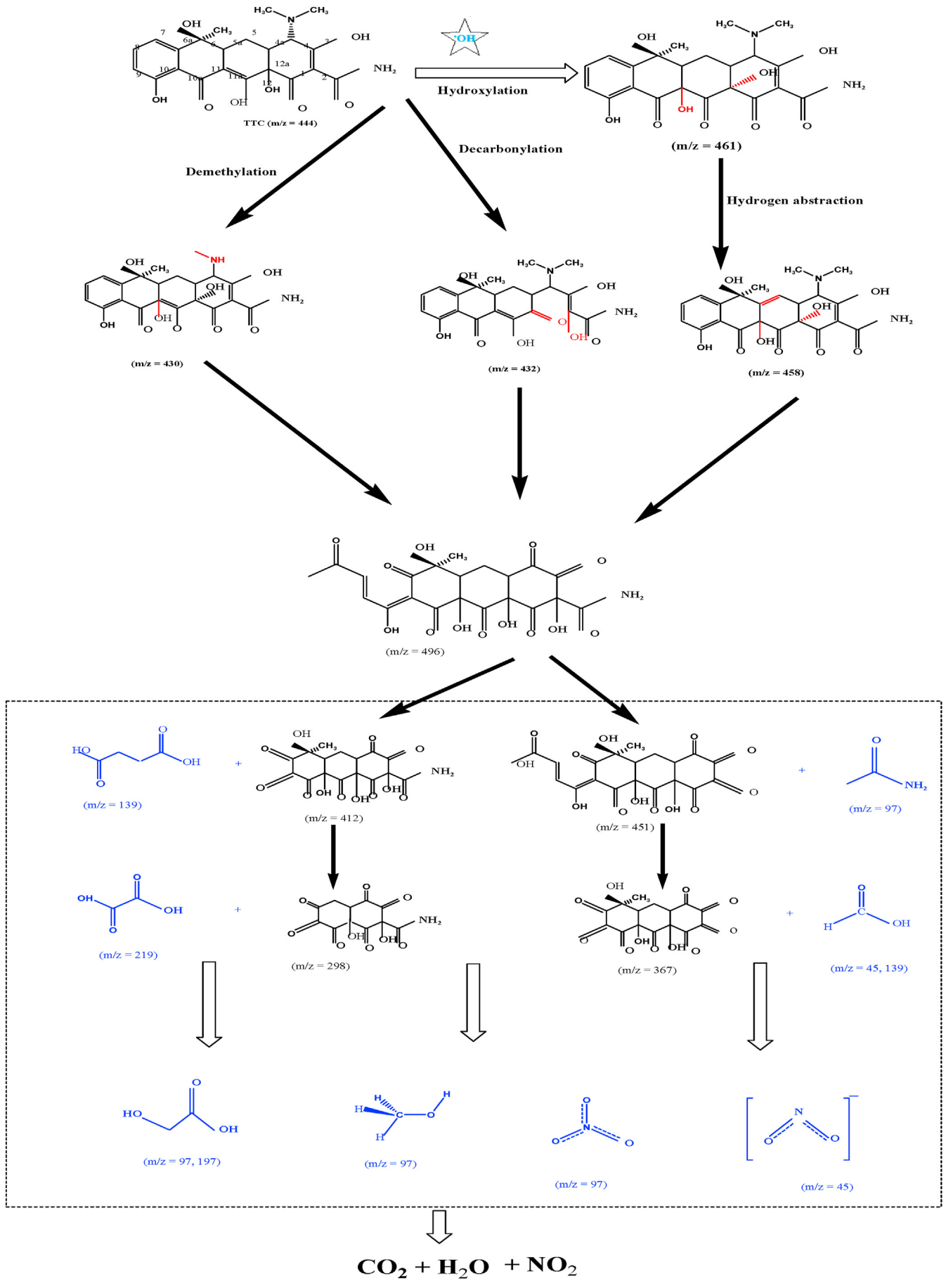
TTC (m/z = 444)
Hydroxylation
(m/z = 461)
Demethylation
Decarbonylation
Hydrogen abstraction
(m/z = 430)
(m/z = 432)
(m/z = 458)
(m/z = 496)
(m/z = 139)
(m/z = 412)
(m/z = 451)
(m/z = 97)
(m/z = 219)
(m/z = 298)
(m/z = 367)
(m/z = 45, 139)
(m/z = 97, 197)
(m/z = 97)
(m/z = 97)
(m/z = 45)
CO2 + H2O + NO2

decarbonylation process, direct •OH attack leads to degradation of the TTC rings. This phenomenon proceeds by firstly destruction of the CO group of TTC via •OH oxidation. Moreover, in the demethylation process, one of $-CH_3$ groups was eliminated because of small bond energy of N–C (Ao et al., 2019). However, it has also been reported that other transformation products with higher m/z of 496, 451, 412, 367 and 298 were also detected in the similar TTC degradation processes (Jeong et al., 2010; Jiao et al., 2008). Nevertheless, these intermediates were not detected in the present study, which could be due to the different reactive agents and other experimental conditions leading to different intermediates and degradation pathways. As shown in Fig. 10, all detected and proposed transformation products ended in the formation of short chain carboxylic acids and simple aliphatic compounds by further oxidation with •OH.

3.12. Influence of the pyrite/H_2O_2 process on cytotoxicity of TTC

The cytotoxicity of raw solutions, and solutions after pyrite/H_2O_2 treatment was evaluated under optimal experimental conditions. As illustrated in Fig. 11a and b, cell viability significantly decreased ($P \leq 0.05$) after TTC exposure in the raw solutions compared to the control group. This deduction was more severe during 48 h. Fig. 11 shows that the TTC outflow (pyrite/H_2O_2 treated TTC solutions) induces less significant toxicity than TTC inflow (initial TTC solution) at all concentrations. This result suggests that TTC molecules at different concentration extremely induce cytotoxicity. However, treating the TTC in the pyrite/H_2O_2 process under optimal condition may lead to the generation of secondary products that significantly have less toxicity to the cells. Therefore, the catalytic behavior of pyrite in conjunction with H_2O_2 is a promising method for detoxification of the hazardous organic pollutants.

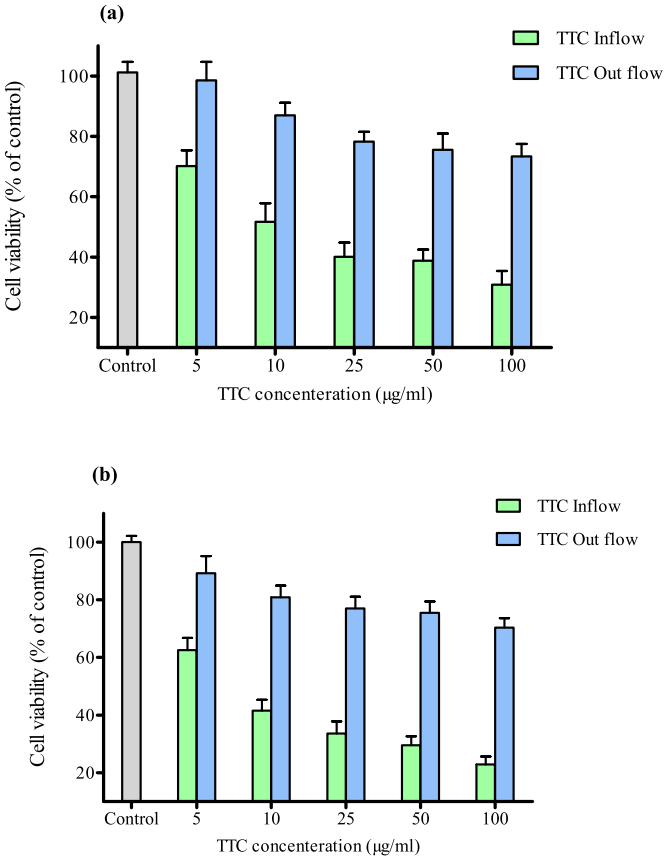

Fig. 11. Effects of various concentration of the raw TTC solution (inflow) and pyrite/H_2O_2-treated TTC solution (out flow) on the viability of the kidney cell lines (a) 24 h and (b) 48 h. Data are presented as mean ± SD from three independent experiments.

4. Conclusion

The efficiency of heterogeneous Fenton-like processes by pyrite originating from mine waste material for the degradation of TTC in aqueous solutions was evaluated and the following conclusions were achieved:

- The pyrite catalyst was prepared from mine debris and analysis indicated that it is a mesoporous powder with a specific surface area of 11.614 m^2/g with a high degree of FeS_2 purity.
- The maximum TTC removal and catalytic efficiency in the pyrite/H_2O_2 process was achieved at a solution pH of 4.1 which is close to the natural pH of the TTC solution (ca. 4.1).
- The results indicated that TTC was mainly degraded through a series of reactions with •OH generated by both attack of H_2O_2 and the surface of pyrite and surface sulfur-defects interaction with H_2O.
- TTC removal was also examined in a common water matrix (in presence of chloride, nitrate and sulfate) and in tap water. The findings demonstrated no considerable inhibitory effects.
- The pyrite/H_2O_2 process acquired comprehensive removal of 50 mg/L TTC and over 85% mineralization during 60 min.
- Pyrite from mine waste sustainable and reusable due to its considerable catalytic activity and low iron leach, even after four successive cycles.
- Short chain carboxylic acids were the main organic intermediates and the nitrogen element present in the TTC molecule is mainly converted to less hazardous species in the degradation process.
- Cytotoxicity tests on raw and pyrite/H_2O_2 treated TTC solutions showed that the cell viability was significantly increased ($P \leq 0.05$) after treatment under optimal conditions.
- Finally, it can be concluded that the H_2O_2 assisted heterogeneous Fenton-like mechanism, using pyrite from mine waste as catalyst, is an effective, promising and cost-effective process for eliminating recalcitrant contaminants from water.

CRediT authorship contribution statement

Ali Mashayekh-Salehi: Conceptualization, Methodology, Software, Formal analysis, Resources, Writing - original draft, Supervision. **Khatare Akbarmojeni:** Investigation, Resources. **Aliakbar Roudbari:** Supervision, Project administration, Resources. **Jan Peter van der Hoek:** Writing - original draft, Visualization. **Ramin Nabizadeh:** Methodology, Software, Data curation. **Mohammad Hadi Dehghani:** Formal analysis, Data curation. **Kamyar Yaghmaeian:** Funding acquisition, Supervision, Project administration.

Declaration of competing interest

The authors declare that they have no known competing financial interests or personal relationships that could have appeared to influence the work reported in this paper.

Fig. 10. Proposed degradation pathways of TTC in the pyrite/H_2O_2 process and the generated transmission products under selected conditions.

Acknowledgment

This research was financially supported by the Department of Environmental Health Engineering, Tehran University of Medical Sciences (TUMH), which is highly appreciated. The authors also gratefully acknowledge the technical support provided by the Department of Environmental Health Engineering, School of Health, Shahroud University of Medical Sciences, Shahroud, Iran.

Appendix A. Supplementary data

Supplementary data to this article can be found online at https://doi.org/10.1016/j.jclepro.2020.125235.

References

Altenor, S., Carene, B., Emmanuel, E., Lambert, J., Ehrhardt, J.J., Gaspard, S., 2009. Adsorption studies of methylene blue and phenol onto vetiver roots activated carbon prepared by chemical activation. J. Hazard Mater. 165, 1029–1039. https://doi.org/10.1016/j.jhazmat.2008.10.133.

American Public Health Association (Apha), 2005. Standard Methods for the Examination of Water and Wastewater, twenty-first ed. American Water Works Association/American Public Works Association/Water Environment Federation, APHA:Washington, DC, USA. https://doi.org/10.2105/AJPH.51.6.940-a. 2005.

Ao, X., Sun, W., Li, S., Yang, C., Li, C., Lu, Z., 2019. Degradation of tetracycline by medium pressure UV-activated peroxymonosulfate process: influencing factors, degradation pathways, and toxicity evaluation. Chem. Eng. J. 361, 1053–1062. https://doi.org/10.1016/j.cej.2018.12.133.

Arzate-Salgado, S.-Y., Morales-Pérez, A.-A., Solís-López, M., Ramírez-Zamora, R.-M., 2016. Evaluation of metallurgical slag as a Fenton-type photocatalyst for the degradation of an emerging pollutant. Diclofenac. Catal. Today 266, 126–135.

Awasthi, M.K., Chen, H., Liu, T., Awasthi, S.K., Wang, Q., Ren, X., Duan, Y., Zhang, Z., 2019. Respond of clay amendment in chicken manure composts to understand the antibiotic resistant bacterial diversity and its correlation with physico-chemical parameters. J. Clean. Prod. 236 https://doi.org/10.1016/j.jclepro.2019.117715.

Bae, S., Kim, D., Lee, W., 2013. Degradation of diclofenac by pyrite catalyzed Fenton oxidation. Appl. Catal. B Environ. 134, 93–102.

Barhoumi, N., Oturan, N., Olvera-Vargas, H., Brillas, E., Gadri, A., Ammar, S., Oturan, M.A., 2016. Pyrite as a sustainable catalyst in electro-Fenton process for improving oxidation of sulfamethazine. Kinetics, mechanism and toxicity assessment. Water Res 94, 52–61.

Bokare, A.D., Choi, W., 2014. Review of iron-free Fenton-like systems for activating H2O2 in advanced oxidation processes. J. Hazard Mater. 275, 121–135.

Borah, D., Senapati, K., 2006. Adsorption of Cd(II) from aqueous solution onto pyrite. Fuel 85, 1929–1934. https://doi.org/10.1016/j.fuel.2006.01.012.

Borda, M.J., Elsetinow, A.R., Strongin, D.R., Schoonen, M.A., 2003. A mechanism for the production of hydroxyl radical at surface defect sites on pyrite. Geochem. Cosmochim. Acta 67, 935–939. https://doi.org/10.1016/S0016-7037(02)01222-X.

Bose, S., Hochella, M.F., Gorby, Y.A., Kennedy, D.W., McCready, D.E., Madden, A.S., Lower, B.H., 2009. Bioreduction of hematite nanoparticles by the dissimilatory iron reducing bacterium Shewanella oneidensis MR-1. Geochem. Cosmochim. Acta 73, 962–976. https://doi.org/10.1016/j.gca.2008.11.031.

Chandra, A.P., Gerson, A.R., 2010. The mechanisms of pyrite oxidation and leaching: a fundamental perspective. Surf. Sci. Rep. 65, 293–315. https://doi.org/10.1016/j.surfrep.2010.08.003.

Charbouillot, T., Brigante, M., Mailhot, G., Maddigapu, P.R., Minero, C., Vione, D., 2011. Performance and selectivity of the terephthalic acid probe for OH as a function of temperature, pH and composition of atmospherically relevant aqueous media. J. Photochem. Photobiol. Chem. 222, 70–76.

Che, H., Bae, S., Lee, W., 2011. Degradation of trichloroethylene by Fenton reaction in pyrite suspension. J. Hazard Mater. 185, 1355–1361.

Chen, S., Xiong, P., Zhan, W., Xiong, L., 2018. Degradation of ethylthionocarbamate by pyrite-activated persulfate. Miner. Eng. 122, 38–43.

Chen, Y.-Y., Ma, Y.-L., Yang, J., Wang, L.-Q., Lv, J.-M., Ren, C.-J., 2017. Aqueous tetracycline degradation by H2O2 alone: removal and transformation pathway. Chem. Eng. J. 307, 15–23.

Cohn, C.A., Laffers, R., Schoonen, M.A.A., 2006. Using yeast RNA as a probe for generation of hydroxyl radicals by earth materials. Environ. Sci. Technol. 40, 2838–2843.

Dhanasekara, S., Attanayake, A.N.B., Herath, A.C., Nanayakkara, N., Senaratne, A., Indrarathne, S.P., Weerasooriya, R., 2015. Partial degradation of carbofuran by natural pyrite. Environ. nanotechnology, Monit. Manag. 4, 51–57.

Diao, Z.-H., Liu, J.-J., Hu, Y.-X., Kong, L.-J., Jiang, D., Xu, X.-R., 2017. Comparative study of Rhodamine B degradation by the systems pyrite/H2O2 and pyrite/persulfate: reactivity, stability, products and mechanism. Separ. Purif. Technol. 184, 374–383.

Duan, Y., Ying, Q., Deng, Y., 2016. REMOVAL of MERCURY from WATER by A REACTIVE ADSORBENT-PYRITE A Dissertation.

Fathinia, S., Fathinia, M., Rahmani, A.A., Khataee, A., 2015. Preparation of natural pyrite nanoparticles by high energy planetary ball milling as a nanocatalyst for heterogeneous Fenton process. Appl. Surf. Sci. 327, 190–200. https://doi.org/10.1016/j.apsusc.2014.11.157.

Feng, Y., Li, H., Lin, L., Kong, L., Li, X., Wu, D., Zhao, H., Shih, K., 2018. Degradation of 1, 4-dioxane via controlled generation of radicals by pyrite-activated oxidants: Synergistic effects, role of disulfides, and activation sites. Chem. Eng. J. 336, 416–426.

Gao, Y., Wang, Y., Zhang, H., 2015. Removal of Rhodamine B with Fe-supported bentonite as heterogeneous photo-Fenton catalyst under visible irradiation. Appl. Catal. B Environ. 178, 29–36.

Ghanbarian, M., Nabizadeh, R., Nasseri, S., Shemirani, F., Mahvi, A.H., Beyki, M.H., Mesdaghinia, A., 2017. Potential of amino-riched nano-structured MnFe2O4@cellulose for biosorption of toxic Cr (VI): modeling, kinetic, equilibrium and comparing studies. Int. J. Biol. Macromol. 104, 465–480.

Giri, A.S., Golder, A.K., 2014. Fenton, photo-fenton, H2O2 photolysis, and TiO2 photocatalysis for dipyrone oxidation: drug removal, mineralization, biodegradability, and degradation mechanism. Ind. Eng. Chem. Res. 53, 1351–1358.

Gosselin, F., Madeira, L.M., Juhna, T., Block, J.C., 2013. Drinking water and biofilm disinfection by Fenton-like reaction. Water Res. 47, 5631–5638.

Groele, J., Foster, J., 2019. Hydrogen peroxide interference in chemical oxygen demand assessments of plasma treated waters. Plasma. https://doi.org/10.3390/plasma2030021.

Hermosilla, D., Cortijo, M., Huang, C.P., 2009. Optimizing the treatment of landfill leachate by conventional Fenton and photo-Fenton processes. Sci. Total Environ. 407, 3473–3481.

Hochi, K., Kubo, T., Sakai, T., Kojima, T., 2016. Sulfur-based Positive-Electrode Active Material and Lithium-Ion Secondary Battery.

Hopkins, Z.R., Blaney, L., 2014. A novel approach to modeling the reaction kinetics of tetracycline antibiotics with aqueous ozone. Sci. Total Environ. 468, 337–344.

Hou, L., Wang, L., Royer, S., Zhang, H., 2016. Ultrasound-assisted heterogeneous Fenton-like degradation of tetracycline over a magnetite catalyst. J. Hazard Mater. 302, 458–467.

Hou, L., Zhang, H., Xue, X., 2012. Ultrasound enhanced heterogeneous activation of peroxydisulfate by magnetite catalyst for the degradation of tetracycline in water. Separ. Purif. Technol. 84, 147–152.

Imoberdorf, G., Mohseni, M., 2011. Degradation of natural organic matter in surface water using vacuum-UV irradiation. J. Hazard Mater. 186, 240–246.

Jeong, J., Song, W., Cooper, W.J., Jung, J., Greaves, J., 2010. Degradation of tetracycline antibiotics: mechanisms and kinetic studies for advanced oxidation/reduction processes. Chemosphere 78, 533–540.

Jiao, S., Zheng, S., Yin, D., Wang, L., Chen, L., 2008. Aqueous photolysis of tetracycline and toxicity of photolytic products to luminescent bacteria. Chemosphere 73, 377–382.

Kang, Y.W., Cho, M.J., Hwang, K.Y., 1999. Correction of hydrogen peroxide interference on standard chemical oxygen demand test. Water Res. https://doi.org/10.1016/S0043-1354(98)00315-7.

Kantar, C., Ari, C., Keskin, S., 2015a. Comparison of different chelating agents to enhance reductive Cr(VI) removal by pyrite treatment procedure. Water Res. 76, 66–75. https://doi.org/10.1016/j.watres.2015.02.058.

Kantar, C., Ari, C., Keskin, S., Dogaroglu, Z.G., Karadeniz, A., Alten, A., 2015b. Cr(VI) removal from aqueous systems using pyrite as the reducing agent: batch, spectroscopic and column experiments. J. Contam. Hydrol. 174, 28–38. https://doi.org/10.1016/j.jconhyd.2015.01.001.

Kantar, C., Oral, O., Oz, N.A., 2019a. Ligand enhanced pharmaceutical wastewater treatment with Fenton process using pyrite as the catalyst: column experiments. Chemosphere 237. https://doi.org/10.1016/j.chemosphere.2019.124440.

Kantar, C., Oral, O., Urken, O., Oz, N.A., 2019b. Role of complexing agents on oxidative degradation of chlorophenolic compounds by pyrite-Fenton process: batch and column experiments. J. Hazard Mater. 373, 160–167. https://doi.org/10.1016/j.jhazmat.2019.03.065.

Kantar, C., Oral, O., Urken, O., Oz, N.A., Keskin, S., 2019c. Oxidative degradation of chlorophenolic compounds with pyrite-Fenton process. Environ. Pollut. 247, 349–361. https://doi.org/10.1016/j.envpol.2019.01.017.

Khabbaz, M., Entezari, M.H., 2017. Degradation of Diclofenac by sonosynthesis of pyrite nanoparticles. J. Environ. Manage. 187, 416–423.

Kharangarh, P.R., Umapathy, S., Singh, G., 2018. Investigation of sulfur related defects in graphene quantum dots for tuning photoluminescence and high quantum yield. Appl. Surf. Sci. 449, 363–370.

Khataee, A., Fathinia, S., Fathinia, M., 2017. Production of pyrite nanoparticles using high energy planetary ball milling for sonocatalytic degradation of sulfasalazine. Ultrason. Sonochem. 34, 904–915.

Khataee, A., Gholami, P., Vahid, B., 2016. Heterogeneous sono-Fenton-like process using nanostructured pyrite prepared by Ar glow discharge plasma for treatment of a textile dye. Ultrason. Sonochem. 29, 213–225.

Kuo, W.G., 1992. Decolorizing dye wastewater with Fenton's reagent. Water Res. https://doi.org/10.1016/0043-1354(92)90192-7.

Labiadh, L., Oturan, M.A., Panizza, M., Hamadi, N. Ben, Ammar, S., 2015. Complete removal of AHPS synthetic dye from water using new electro-fenton oxidation catalyzed by natural pyrite as heterogeneous catalyst. J. Hazard Mater. 297, 34–41. https://doi.org/10.1016/j.jhazmat.2015.04.062.

Lee, E., Lee, H., Kim, Y.K., Sohn, K., Lee, K., 2011. Hydrogen peroxide interference in chemical oxygen demand during ozone based advanced oxidation of anaerobically digested livestock wastewater. Iran. J. Environ. Heal. Sci. Eng.

Li, J., Zheng, X., Liu, K., Sun, S., Li, X., 2016. Effect of tetracycline on the growth and nutrient removal capacity of Chlamydomonas reinhardtii in simulated effluent from wastewater treatment plants. Bioresour. Technol. 218, 1163–1169.
Li, S., Hu, J., 2016. Photolytic and photocatalytic degradation of tetracycline: effect of humic acid on degradation kinetics and mechanisms. J. Hazard Mater. 318, 134–144.
Lian, W., Yi, X., Huang, K., Tang, T., Wang, R., Tao, X., Zheng, Z., Dang, Z., Yin, H., Lu, G., 2019. Degradation of tris (2-chloroethyl) phosphate (TCEP) in aqueous solution by using pyrite activating persulfate to produce radicals. Ecotoxicol. Environ. Saf. 174, 667–674.
Liang, C., Su, H.-W., 2009. Identification of sulfate and hydroxyl radicals in thermally activated persulfate. Ind. Eng. Chem. Res. 48, 5558–5562.
Liu, J., Zhong, S., Song, Y., Wang, B., Zhang, F., 2018. Degradation of tetracycline hydrochloride by electro-activated persulfate oxidation. J. Electroanal. Chem. 809, 74–79.
Loeb, B.L., 2009. Ozone: science & engineering thirty years of progress. Ozone Sci. Eng. 31, 379–392.
López-Peñalver, J.J., Sánchez-Polo, M., Gómez-Pacheco, C.V., Rivera-Utrilla, J., 2010. Photodegradation of tetracyclines in aqueous solution by using UV and UV/H2O2 oxidation processes. J. Chem. Technol. Biotechnol. 85, 1325–1333.
Ma, C.-H., Wang, L., Yan, Y.-S., Che, G.-B., Yin, Y.-S., Wang, R.-Z., Li, D.-Y., 2009. Extraction of tetracycline via ionic liquid two-phase system. Chem. Res. Chin. Univ. 25, 832–835.
Mackuľak, T., Mosný, M., Grabic, R., Golovko, O., Koba, O., Birošová, L., 2015. Fenton-like reaction: a possible way to efficiently remove illicit drugs and pharmaceuticals from wastewater. Environ. Toxicol. Pharmacol. 39, 483–488.
Mashayekh-Salehi, A., Moussavi, G., Yaghmaeian, K., 2017. Preparation, characterization and catalytic activity of a novel mesoporous nanocrystalline MgO nanoparticle for ozonation of acetaminophen as an emerging water contaminant. Chem. Eng. J. 310 https://doi.org/10.1016/j.cej.2016.10.096.
Mboula, V.M., Hequet, V., Gru, Y., Colin, R., Andres, Y., 2012. Assessment of the efficiency of photocatalysis on tetracycline biodegradation. J. Hazard Mater. 209, 355–364.
Mirzaei, A., Chen, Z., Haghighat, F., Yerushalmi, L., 2017. Removal of pharmaceuticals from water by homo/heterogonous Fenton-type processes–A review. Chemosphere 174, 665–688.
Moussavi, G., Khosravi, R., Omran, N.R., 2012. Development of an efficient catalyst from magnetite ore: characterization and catalytic potential in the ozonation of water toxic contaminants. Appl. Catal. Gen. https://doi.org/10.1016/j.apcata.2012.08.002.
Moussavi, G., Mashayekh-Salehi, A., Yaghmaeian, K., Mohseni-Bandpei, A., 2018a. The catalytic destruction of antibiotic tetracycline by sulfur-doped manganese oxide (S–MgO) nanoparticles. J. Environ. Manag. 210, 131–138. https://doi.org/10.1016/j.jenvman.2018.01.004.
Moussavi, G., Pourakbar, M., Aghayani, E., Mahdavianpour, M., 2018b. Investigating the aerated VUV/PS process simultaneously generating hydroxyl and sulfate radicals for the oxidation of cyanide in aqueous solution and industrial wastewater. Chem. Eng. J. 350, 673–680.
Moussavi, G., Pourakbar, M., Aghayani, E., Mahdavianpour, M., Shekoohyian, S., 2016. Comparing the efficacy of VUV and UVC/S2O82-advanced oxidation processes for degradation and mineralization of cyanide in wastewater. Chem. Eng. J. 294, 273–280.
Nidheesh, P.V., 2015. Heterogeneous Fenton catalysts for the abatement of organic pollutants from aqueous solution: a review. RSC Adv. 5, 40552–40577.
Niu, H., Meng, Z., Cai, Y., 2012. Fast defluorination and removal of norfloxacin by alginate/Fe@ Fe3O4 core/shell structured nanoparticles. J. Hazard. Mater. 227, 195–203.
Okoli, C.P., Ofomaja, A.E., 2019. Development of sustainable magnetic polyurethane polymer nanocomposite for abatement of tetracycline antibiotics aqueous pollution: response surface methodology and adsorption dynamics. J. Clean. Prod. 217, 42–55. https://doi.org/10.1016/j.jclepro.2019.01.157.
Oral, O., Kantar, C., 2019. Diclofenac removal by pyrite-Fenton process: performance in batch and fixed-bed continuous flow systems. Sci. Total Environ. 664, 817–823. https://doi.org/10.1016/j.scitotenv.2019.02.084.
Oral, O., Urken, O., Kantar, C., Kaplan, I., Ayman Oz, N., 2017. Reaction mechanisms associated with oxidative chlorophenol degradation by modified fenton process using pyrite as the catalyst. Geophys. Res. Abstr.
Peng, S., Feng, Y., Liu, Y., Wu, D., 2018. Applicability study on the degradation of acetaminophen via an H2O2/PDS-based advanced oxidation process using pyrite. Chemosphere 212, 438–446.
Pereira, J.F.B., Vicente, F., Santos-Ebinuma, V.C., Araújo, J.M., Pessoa, A., Freire, M.G., Coutinho, J.A.P., 2013. Extraction of tetracycline from fermentation broth using aqueous two-phase systems composed of polyethylene glycol and cholinium-based salts. Process Biochem. 48, 716–722.
Pham, H.T., Kitsuneduka, M., Hara, J., Suto, K., Inoue, C., 2008. Trichloroethylene transformation by natural mineral pyrite: the deciding role of oxygen. Environ. Sci. Technol. 42, 7470–7475.
Pourakbar, M., Moussavi, G., Shekoohiyan, S., 2016. Homogenous VUV advanced oxidation process for enhanced degradation and mineralization of antibiotics in contaminated water. Ecotoxicol. Environ. Saf. 125, 72–77.
Qiao, J., Zhang, H., Li, G., Li, S., Qu, Z., Zhang, M., Wang, J., Song, Y., 2019. Fabrication of a novel Z-scheme SrTiO3/Ag2S/CoWO4 composite and its application in sonocatalytic degradation of tetracyclines. Separ. Purif. Technol. 211, 843–856.
Rahim Pouran, S., Abdul Raman, A.A., Wan Daud, W.M.A., 2014. Review on the application of modified iron oxides as heterogeneous catalysts in Fenton reactions. J. Clean. Prod. https://doi.org/10.1016/j.jclepro.2013.09.013.
Raut-Jadhav, S., Badve, M.P., Pinjari, D.V., Saini, D.R., Sonawane, S.H., Pandit, A.B., 2016. Treatment of the pesticide industry effluent using hydrodynamic cavitation and its combination with process intensifying additives (H2O2 and ozone). Chem. Eng. J. https://doi.org/10.1016/j.cej.2016.03.019.
Ravikumar, K.V.G., Sudakaran, S.V., Ravichandran, K., Pulimi, M., Natarajan, C., Mukherjee, A., 2019. Green synthesis of NiFe nano particles using Punica granatum peel extract for tetracycline removal. J. Clean. Prod. 210, 767–776. https://doi.org/10.1016/j.jclepro.2018.11.108.
Reyes, C., Fernández, J., Freer, J., Mondaca, M.A., Zaror, C., Malato, S., Mansilla, H.D., 2006. Degradation and inactivation of tetracycline by TiO2 photocatalysis. J. Photochem. Photobiol. Chem. https://doi.org/10.1016/j.jphotochem.2006.04.007.
Schoonen, M.A.A., Harrington, A.D., Laffers, R., Strongin, D.R., 2010. Role of hydrogen peroxide and hydroxyl radical in pyrite oxidation by molecular oxygen. Geochem. Cosmochim. Acta 74, 4971–4987.
Shaida, M.A., Sen, A.K., Dutta, R.K., 2018. Alternate use of sulphur rich coals as solar photo-Fenton agent for degradation of toxic azo dyes. J. Clean. Prod. 195, 1003–1014. https://doi.org/10.1016/j.jclepro.2018.05.286.
Shariati, S., Yamini, Y., Esrafili, A., 2009. Carrier mediated hollow fiber liquid phase microextraction combined with HPLC–UV for preconcentration and determination of some tetracycline antibiotics. J. Chromatogr. B 877, 393–400.
Sharma, J., Mishra, I.M., Kumar, V., 2015. Degradation and mineralization of Bisphenol A (BPA) in aqueous solution using advanced oxidation processes: UV/H2O2 and UV/S2O82− oxidation systems. J. Environ. Manag. 156, 266–275.
Shi, X., Tian, A., You, J., Yang, H., Wang, Y., Xue, X., 2018. Degradation of organic dyes by a new heterogeneous Fenton reagent-Fe2GeS4 nanoparticle. J. Hazard. Mater. 353, 182–189.
Sun, Y., Lv, D., Zhou, J., Zhou, X., Lou, Z., Baig, S.A., Xu, X., 2017. Adsorption of mercury (II) from aqueous solutions using FeS and pyrite: a comparative study. Chemosphere 185, 452–461. https://doi.org/10.1016/j.chemosphere.2017.07.047.
Talinli, I., Anderson, G.K., 1992. Interference of hydrogen peroxide on the standard cod test. Water Res. https://doi.org/10.1016/0043-1354(92)90118-N.
Titouhi, H., Belgaied, J.-E., 2016. Heterogeneous Fenton oxidation of ofloxacin drug by iron alginate support. Environ. Technol. 37, 2003–2015.
Velichkova, F., Julcour-Lebigue, C., Koumanova, B., Delmas, H., 2013. Heterogeneous Fenton oxidation of paracetamol using iron oxide (nano) particles. J. Environ. Chem. Eng. 1, 1214–1222.
Wang, J., Zhi, D., Zhou, H., He, X., Zhang, D., 2018. Evaluating tetracycline degradation pathway and intermediate toxicity during the electrochemical oxidation over a Ti/Ti4O7 anode. Water Res. 137, 324–334.
Wang, S., Wang, J., 2018. Radiation-induced degradation of sulfamethoxazole in the presence of various inorganic anions. Chem. Eng. J. 351, 688–696.
Wols, B.A., Hofman-Caris, C.H.M., 2012. Review of photochemical reaction constants of organic micropollutants required for UV advanced oxidation processes in water. Water Res. 46, 2815–2827.
Wolters, A., Steffens, M., 2005. Photodegradation of antibiotics on soil surfaces: laboratory studies on sulfadiazine in an ozone-controlled environment. Environ. Sci. Technol. 39, 6071–6078.
Wu, J., Zhang, H., Oturan, N., Wang, Y., Chen, L., Oturan, M.A., 2012. Application of response surface methodology to the removal of the antibiotic tetracycline by electrochemical process using carbon-felt cathode and DSA (Ti/RuO2–IrO2) anode. Chemosphere 87, 614–620.
Xu, X.-R., Li, X.-Y., 2010. Sorption and desorption of antibiotic tetracycline on marine sediments. Chemosphere 78, 430–436.
Yaghmaeian, K., Moussavi, G., Mashayekh-Salehi, A., Mohseni-Bandpei, A., Satari, M., 2017. Oxidation of acetaminophen in the ozonation process catalyzed with modified MgO nanoparticles: effect of operational variables and cytotoxicity assessment. Process Saf. Environ. Protect. 109 https://doi.org/10.1016/j.psep.2017.04.020.
Yang, X., Zhang, X., Wang, Z., Li, S., Zhao, J., Liang, G., Xie, X., 2019. Mechanistic insights into removal of norfloxacin from water using different natural iron ore – biochar composites: more rich free radicals derived from natural pyrite-biochar composites than hematite-biochar composites. Appl. Catal. B Environ. 255 https://doi.org/10.1016/j.apcatb.2019.117752.
Zeng, L., Gong, J., Dan, J., Li, S., Zhang, J., Pu, W., Yang, C., 2019. Novel visible light enhanced Pyrite-Fenton system toward ultrarapid oxidation of p-nitrophenol: Catalytic activity, characterization and mechanism. Chemosphere 228, 232–240.
Zhang, P., Yuan, S., Liao, P., 2016. Mechanisms of hydroxyl radical production from abiotic oxidation of pyrite under acidic conditions. Geochem. Cosmochim. Acta 172, 444–457. https://doi.org/10.1016/j.gca.2015.10.015.
Zhang, Y., Zhang, K., Dai, C., Zhou, X., 2014. Performance and mechanism of pyrite for nitrobenzene removal in aqueous solution. Chem. Eng. Sci. 111, 135–141.
Zhu, X.-D., Wang, Y.-J., Sun, R.-J., Zhou, D.-M., 2013. Photocatalytic degradation of tetracycline in aqueous solution by nanosized TiO2. Chemosphere 92, 925–932.
Zou, X., Zhou, T., Mao, J., Wu, X., 2014. Synergistic degradation of antibiotic sulfadiazine in a heterogeneous ultrasound-enhanced Fe0/persulfate Fenton-like system. Chem. Eng. J. 257, 36–44.